

O B S E R V A T I O N S S U P P O R T I N G T H E E X I S T E N C E O F A N I N T R I N S I C M A G N E T I C M O M E N T I N S I D E T H E C E N T R A L C O M P A C T O B J E C T W I T H I N T H E Q U A S A R Q 0 9 5 7 + 5 6 1

Rudolph E. Schild¹, Darryl J. Leiter², and Stanley L. Robertson³

A B S T R A C T

Recent auto-correlation and fluctuation analysis of the time series data in the brightness curves and micro-lensing size scales seen in Q 0957+ 561 A, B has produced important information about the existence and characteristic physical dimensions of a new non-standard internal structure contained within this quasar. We find that the new internal quasar structure, which we shall call the Schild-Vakulik Structure, can be consistently explained in terms of a new class of gravitationally collapsing solutions to the Einstein field equations which describe highly redshifted, Eddington limited, Magnetospheric, Eternally Collapsing Objects (M E C O) that contain intrinsic magnetic moments. Since observation of the Schild-Vakulik structure within Q 0957+ 561 implies that this quasar contains an observable intrinsic magnetic moment, this represents strong evidence that this quasar does not have an event horizon.

Subject headings: Galaxies: Quasars: structure: individual: Q 0957+ 561 | accretion discs: magnetic fields | black hole physics | gravitational lensing: microlensing

1. Introduction

Analyis of gravitational microlensing observations of the quasar Q 0957+ 561 (Schild and Vakulik, 2003; Schild, 2005) has offered strong evidence for the existence of an intrinsic structure within this quasar that can be only be explained by a non-standard luminous quasar model consisting of a thin accretion disc whose interior is essentially empty of

¹Center for Astrophysics, 60 Garden Street, Cambridge, MA 02138

²FSTC, Charlottesville, VA 22901

³Dept. of Physics, Southwestern Oklahoma State University, Weatherford, OK 73096

matter out to a luminous inner edge which resides at about 70 gravitational radii from the central compact object, and which is also surrounded by an order of magnitude larger outer ring-shaped Elvis Structure where the broad blue-shifted emission lines are formed. While this non-standard form of inner quasar structure (which we shall call the Schild-Vakulik Structure) was shown to have the remarkable property of being able to explain all of the observed features of Q 0957 obtained from 24 years of gravitational microlensing, the physical origin and interpretation of this exotic inner quasar structure remained an unsolved mystery.

During the same time period that the gravitational microlensing based discovery of the Schild-Vakulik structure in quasar Q 0957 occurred, the related discovery of a new paradigm in astrophysics based on X-ray and Radio Astronomy data had begun to emerge. This new paradigm came in the form of four sequentially published papers which presented strong observational and theoretical evidence in support of the idea that both galactic black hole candidates (G B H C) and Active Galactic Nuclei A G N have observable intrinsic magnetic moments.

This latter discovery was revealed in the following manner: a) First it was argued (Robertson and Leiter, 2002) that the spectral state switch and quiescent luminosities of low mass x-ray binaries, (LM X B) including G B H C, can be well explained by a magnetic propeller effect that requires an intrinsically magnetized central object. b) Second it was shown (Leiter and Robertson, 2003; Robertson and Leiter, 2003) that this result was consistent with the existence of a new class of gravitationally collapsing solutions of the Einstein field equations in General Relativity which describe highly redshifted, Magnetospheric, Eternally Collapsing Objects (M E C O) that do not have trapped surfaces leading to event horizons.

These general relativistic M E C O solutions were shown to emerge from the physical requirement that the structure and radiation transfer properties of the energy-momentum tensor on the right hand side of the Einstein field equations for a collapsing object must contain equipartition magnetic fields that generate a highly redshifted Eddington limited secular collapse process which satisfies the Strong Principle of Equivalence (S P E) requirement of time like world line completeness.

Finally it was demonstrated (Robertson and Leiter, 2004) that G B H C and A G N modeled as intrinsically magnetic M E C O objects can produce jets that emit radio-infrared luminosity correlated with mass and x-ray luminosity in a manner which correctly predicts the observed exponent, mass scale invariant cutoff, and radio luminosity ratios of both G B H C and A G N. In the following sections we show that the two different lines of research discussed above converge in a manner allowing the construction of a logical chain of

observational and theoretical arguments which solves the mystery of the physical origin of the Schild-Vakulik structure observed within the quasar Q 0957. In order to do this we use the Magnetospherical Eternally Collapsing Object (M ECO) paradigm (discussed in detail in the Appendices of this paper) as a model to interpret the physical meaning of the gravitational micro-lensed Schild-Vakulik structure seen in Q 0957.

In this context we show that the Schild-Vakulik structure actually represents the key observable dynamical signature of a 3.6 billion solar mass M ECO acting as the central compact object in this quasar instead of a black hole. Hence we are led to conclude that the observation of the Schild-Vakulik structure within Q 0957 represents strong evidence that this quasar does not have an event horizon.

2. Quasar Structure Size Estimates from Brightness Time Series Auto-correlation

The most accurate direct measurement available of the inner quasar size is in the long time series brightness data collected over many years to study the gravitational lens time delay and micro-lensing. Evidence for the outer ring (Elvis) structures in this data set has already been discussed by Schild (2005) from analysis of the internally created repetitions seen in the long brightness record.

In addition an inner structure has also been discussed in Schild (2005) and in previous references. Heretofore it has been discussed as the "luminous inner edge of the accretion disc" according to standard ideas of quasar structure dominated by a black hole surrounded by an accretion disc and perhaps outer clouds or Elvis outer structures. However recent more accurate numerical estimates of the size of the inner quasar structure of Q 0957 have implied that its size is actually larger than previously estimated and for this reason better explained as the luminous ring expected at the magnetospheric radius of an empirical quasar model in which the central compact object in the quasar is dominated by the dynamical effects of an intrinsic magnetic propeller acting in this sensitive inner region.

This improved more accurate empirical quasar model for Q 0957+561 has been found to be most consistently explained in the context of the recently discovered new class of gravitationally collapsing solutions to the Einstein field equations which describe compact gravitationally collapsing object in terms of highly red shifted, Magnetospheric, Eternally Collapsing Objects (M ECO) that do not have trapped surfaces leading to event horizons. In the following paragraphs, in order to help the reader of this paper maintain the continuity and flow of the observational arguments which support the above conclusions, the specific

details about the M ECO model and the published articles associated with it have been put into a series of short appendices (Appendix 1-10) and will be referred to when needed in order to clarify the details of specific calculations associated with the observational data.

We now begin discussing the observational arguments referred to above by first noting that two manifestations of the dynamical inner structure of Q 0957+561 A, B have been seen: 1. Direct auto-correlation calculations of the brightness record for the two image components have revealed an inner structure with an associated time scale of approximately 10 days (Schild 2005). 2. Time delay calculations by several research groups have indicated that several time delays seem to be present. In particular, in addition to the now firmly established 417.1 day time delay (Colley et al 2003) there is convincing evidence for lags of 404 days (Schild, 1991; Thomson and Schild 1997) and 424 days (Pijpers 1997, Osoz et al 2002, Pelt et al 1996). It is likely that these lags caused by internal structure are part of the reason why it has been so difficult to determine the cosmological time delay. Regarding 2 above, recall that the time delay controversy in the 1990's era was probably a manifestation of quasar structure causing several lags to produce cross-correlation peaks that can also create spurious cross-correlation peaks.

Recall that the difference between the 404-day concurrent time delay value (Schild 1991; Thomson and Schild 1997) and the erroneous Press et al (1992) value of 534 days is exactly the 129 day value found as an auto-correlation peak illustrated in Fig. 1 of Schild 2005. The existence of internal rejections/ fluorescence as manifestations of internal quasar structure can easily be seen in the most recent Q 2237 data available at: <http://www.astrowu.edu.pl/ogle/ogle3/huchra.htm>. Here we see that the intrinsic quasar fluctuation seen as a sudden brightening of all four quasar images at HJD -2450000 = 2900 was again seen at 3230, or 330 days later (observer's clock); correction for redshift of 1.69 gives a proper lag of 123 days, which is comparable to the lags seen in Q 0957 as found in Schild (2005). Thus the two gravitational lenses with adequate data show the complex behavior that an intrinsic fluctuation is seen at multiple times, almost certainly betraying the existence of complex internal quasar structure that can confound time delay determination but that also provides important clues about the structure of the quasar. Existence of multiple lags caused by quasar internal structure also allows us to estimate the size of the inner edge of the accretion disc, using methodology and results from Schild 2005. We assume that the cosmological time delay is 417.1 days (Colley et al 2003) but that the internal quasar structure also produces lags at t_1 and t_2 following the initial impulse.

Thus the impulse seen in the first arriving A image will correlate strongly with the second arriving B image at lags of 417, $417+t_1$, and $417+t_2$ days. Of course there should be strong correlation at $417+t_2$ and $417+t_1$ days due to secondary impulses contained in the

A (rst arriving) in age. Evidence for these lags shorter than the cosmological time delay has been reported in Schild and Thomson (1997) who note that "this calculation produces a broad maximum with an absolute peak for 387-day lag. Note that the calculation produces a number of peaks near 400 days, and the peaks have a uniform spacing of 16 days, which may correspond to an internal rection within the inner quasar structure ..." Because the hot inner radius of the accretion disk will be seen as the small brightness enhancement for 2 lags corresponding to the ring radius and for the known inclination, we ask if the measured lags for the 404 and 424 day measured delays follow from the Schild (2005) model and geometry in Q0957. The answer is an unqualified yes. The shortest lag, 7 days observed (ie, 424 – 417 days) must correspond to the interaction (refection) from the near side of the ring. Then the refection from the far side must be at 13 days, which is both the lag measured (ie, 417 – 404 days) and the lag predicted given the preferred case 1 geometry of Schild 2005.

In other words, given the quasar inclination measured from the Elvis structures, and given one of the measured inner ring lags, we can predict the second (measured, 13-day) inner ring lag. This quasar structure and its interpretation is necessarily complicated because the effects of the solar mass micro-lensing star must selectively magnify the 2 sides of the inner edge of the accretion disk differently at different times. While this produces complexity in interpretation, it also generates information about the direction of motion of the micro-lensing star in the lens galaxy G1. Finally, from this complex chain of analysis of internal quasar structure, we determine the size of the luminous inner edge of the accretion disk. For the geometrical factors of the model as determined above, the measured 424-day and 404-day lags combined with a 417.1-day cosmological time delay (Colley et al 2003) and correction for the 54 degree inclination of the quasar's pole from the line of sight (Schild 2005) gives an a rather large value for the inner radius of the accretion disk of $(3.9 \pm 0.16) \times 10^{16}$ cm, where the error is estimated from the 1-day discreteness of the reported lags and the averaging of the two estimates from the above two lag determinations.

3. Empirical Estimates of the Thickness of The Hot Annular Ring Observed To Occur At The Inner Radius of The Accretion Disk

The inner radius of the accretion disk (which will later be associated with the MECO magnetospheric radius) is considered to be the smallest observable structure in the Q0957 quasar and therefore the rapid fluctuations observed by Colley and Schild (2003) are presumed to originate there. However it is not yet clear by what mechanism the brightness fluctuations are produced. We consider the two most probable mechanisms; micro-lensing

or changes in the quasar structure. The most critical observations defining a lower size limit are seen in the CS03 data, which seem to demonstrate rapid brightness fluctuations of 1 percent amplitude and 12 hour duration in both the intrinsic quasar brightness fluctuations and in the microlensing.

We refer to the patterns of fluctuations shown in Fig. 1 of CS03. There, on Julian Dates 2449701 – 05 we see a pattern of fluctuations which was seen the first year of observations in image A (filled dots) and after a 417-day time delay, seen in image B (open circles). The brightness trend seems to show convincingly that a pattern of intrinsic fluctuations was seen, with several brightness changes of approximately 1 percent with a time lag on the order of 12 hours. Thus in day 1, the quasar appears to have declined in brightness by .017 magnitudes in 0.43 days (solid line fitted to the data points in the upper panel). Note that this must be an intrinsic quasar brightness fluctuation, because it is seen in both the first- and second-arriving images. In addition, microlensing fluctuations of comparable amplitude must exist, as again illustrated in Fig. 1 of CS03. Referring to the data for Julian Day 2449706, we can see from the many time-overlapping points that the quasar image brightness does not agree for this date, and the difference between the two observations for the same proper quasar time shows the profile illustrated in the lower panel of Fig. 1, where a microlensing event with 12 hour time scale and .01 magnitude amplitude is detected. Because this profile must originate in microlensing, it would be expected to have a cusp-shaped profile unless the source structure is partially resolved, as seems to be observed here.

These simple amplitude and time-scale estimates of microlensing and intrinsic quasar brightness changes are entirely compatible with previously published estimates, expressed as wavelet amplitude (Schild 1999), structure function (Colley and Schild 1999), and Fourier power spectrum (Thomson and Schild 1997). [include a quote from a manuscript] The wavelet fits to the A and B images separately (Schild 1999) measure the total amplitude in fluctuations independently of whether the fluctuations originate in intrinsic or microlensing variability. Nevertheless the amplitudes measured for the A and B images are seen in Schild 1999 Fig. 8 to be of amplitude 1% on time scales of 2 days in the mean. The event of CS03 is exceptionally by a factor of 4 in time, but this is of course a probable selection effect. The view that these most rapid low amplitude fluctuations originate in the inner ring of the accretion disk produces a new view of the nature and origin of the quasar luminous signal and its microlensing.

If we adopt for the moment a model of the inner quasar where a disturbance of some kind, perhaps related to ingestion of a mass unit, and seen throughout the inner corona and its surrounding inner ring of the accretion disk, then we would expect to see the brightness

enhancement signaling this event originate in the corona and again, after short lags of order of days, when the event is seen in the nearer and then the farther sides of the inner ring of the accretion disk. Because each of these regions will be microlensed independently and differently, it would be unsurprising if the micro-lensing had the same amplitudes and time scales for brightness fluctuations as the intrinsic brightness fluctuations, as observed. This important possible kind of micro-lensing is significantly different from the simpler view that the fluctuations are just caused by luminous elements crossing the caustic pattern originating in the lens galaxy (Gould and Miralda-Escude, 1997; Rauch and Blandford 1991). However our new approach requires the quasar to have very fine structure, whose size we now estimate.

3.1. Estimation of Source and Micro-Lensing Amplitudes and Their Time Scales

We estimate first the dimensions implied if we adopt the simple argument that for a significant brightness fluctuation to occur, something must be altering its physical properties and therefore its luminosity on a time sufficiently long that the observed coherence does not violate the principle of causality (meaning that the event is limited in size by the velocity of light). Thus the proper scale of the quasar emitting region that coherently changed its luminosity 5% (because dilution by the steady luminous emission of the large outer Elvis structures produces 80% of the observed quasar brightness according to SV03) is at least as large as the light travel distance, $c t$. For the CS03 event with observed time 12 hours, and proper time $12/2.41$ hours = 5 hours, the probable diameter of the coherent light emitting region is $5 \cdot 4 \cdot 10^{14}$ cm. The numerical value of this length, estimated from coherent brightness fluctuations, represents the radial thickness of the hot annular band at the inner radius of the accretion disk.

3.2. Micro-lensing By Luminous Matter Passing Behind Micro-lensing Cusps

3.2.1 In-fall case

A second estimate of fluctuation source size comes from the model that the fluctuation is due to some luminous unit crossing a cusp originating in the lens galaxy. As already noted by Schild (1996), the cusp pattern would be produced by planetary mass micro-lensing objects, which amplify the shear introduced by the stars also known to be in the lens galaxy, but inferred not to be sufficient to be the baryonic dark matter. This process has already

been modeled by SV03 from which we can adopt some principal results. In SV03 the shear due to solar mass stars is modeled as originating in a population with 0.1 solar mass, but this adopted value is not expected to appreciably affect results since the planetary mass population produces a very significantly finer cusp pattern with a factor 10 larger optical depth. The model adopts standard values for cosmology and for the transverse velocity. A principal result of the model is that the micro-lensing brightness fluctuations that would be observed should be typically .01 magnitudes on a time scale of 10 days (observer's clock), for an adopted thickness of the inner ring of 2×10^{14} cm and for $10^5 M_{\odot}$ micro-lensing particles. This fluctuation time varies as the size of the emitting region and as the square of the micro-lens mass. Thus the structure size scale estimated would be 10^{13} cm and the mass would be $10^7 M_{\odot}$ for the somewhat resolved micro-lensing event found in CS03.

We find it unlikely that the Q0957 quasar has coherent structure on such small size scales, because the brightness fluctuations have no hint of it, although it is possible that an ingested mass unit powering the quasar does. Based on the above discussion, we adopt for now the more conservative conclusion that the observed rapid brightness fluctuations result from a local brightness change in the accretion disk seen at multiple epochs.

3.2.2 Micro-lensing By Orbiting Luminous Material Generated by Magnetospheric Effects

Another micro-lensing scenario has been suggested by Gould and Miralda-Escude (1997) and previously by Rauch and Blandford (1991). In this scenario, orbiting blobs created in the magnetospheric ring region of the inner accretion disc, e.g. like that described by the Magnetically Arrested Disk (MAD) model (Igumenshchev, Narayan, and Abramowicz, 2003) would pass behind the cusp pattern originating in the lens galaxy. However, to be visible, such blobs would necessarily have to have a luminosity comparable to that of the quasar coming from a volume with the diameter of the sun. Furthermore, these luminous blobs would tend to make asymmetric brightness profiles, characterized by successive brightness peaks only, contrary to the wavelet result by Schild (1999) that equal positive and negative fluctuations are found. Furthermore, the mechanism would produce highly periodic brightness effects not observed in any of the lensed quasar systems. Hence we consider this mechanism to be not an important indicator of the quasar structure in Q0957 (for more details on this issue see the theoretical analysis discussion in section 7 below).

4. Structure Function Estimates Inferred From Long Term Brightness Fluctuations

With the shortest time scale brightness fluctuations understood to be indicative of the thickness of the hot inner annulus of the accretion disk in Q 0957+ 561, we consider next the properties of brightness fluctuations observed on longer time scales. The increased amplitudes of brightness fluctuations on longer time scales is often described as the structure function, where amplitude of fluctuation expressed by some measure such as rms deviation, as a function of the interval of time between successive samples of this fluctuating quantity.

Estimates of the structure function have been given for time scales of 1 day to years in Colley and Schild (1998), or in a wavelet calculation and representation by Schild (1999), and also as a Fourier representation of the micro-lensing component (Schild 1996, Fig. 4; Thomson and Schild 1997.) This last reference considers only fluctuations on long time scales, approximately 100 days, and will not here be considered further. In the direct structure function estimates of CS03 and Colley and Schild, 1998, the variance quantity plotted is the square of the brightness difference amplitude as a function of lag between brightness samples. Thus for the plotted t in Fig. 5 of Colley and Schild (2000), the mean fluctuation amplitude for 1-day lag is 0.0063 mag, and the square root of the variance is proportional to the lag. In other words, the mean brightness increase expressed as a rms, is a linear function of lag time.

The same information has been gleaned from a wavelet analysis of the A and B image brightness records as described in Schild 1999. There we report in Figs. 5 and 6 the wavelet amplitude expressed as a mean absolute deviation, and in Figs. 7 and 8 the amplitude expressed as an rms deviation, which is comparable to the presentation in Colley and Schild (2000). The results agree well, with the rms deviation extrapolated to 1 day lag of 0.005 mag, and a linear trend of rms deviation increasing with lag for lags up to approximately 20 days. This linear increase in the structure function is significant and has never been interpreted in the context of a physical process, probably because it has heretofore been anomalous and unexpected. Standard accretion disc models would adopt a simple picture that a disturbance in the accretion disc limited by the causality principle, with the amount of the brightness change increasing with time as the disturbance spreads, would produce a structure function that increases with the square of the time scale for an optically thick accretion disc where the observed optical disturbance increases as the area within causality, or as the cube for the optically thin case.

The observed linear increase is, however, compatible with the MECO quasar model discussed in section 7, where the emitting source is seen as a "annular band" around the equator of the compact object, with the band "thickness" or cross-section diameter of

5.4×10^{14} cm, as estimated above. As the disturbance propagates along the length of the band, the causally connected area increases linearly. However, note that the linear increase should end when the entire length is in causal connection; this occurs when light has traveled a distance of 30 proper light days, the ring diameter, corresponding to an elapsed time of 14 light days (in the observer's frame) when allowance is made for cosmological effects (the $[1+z]$ correction to time) and for geometric effects related to the orientation of the quasar. Thus the "events" seen in wavelet representation would produce up to 16-day wavelets. This 16-day limit may be present in the measured wavelet amplitudes, Figs 5,6,7, and 8 of Schild 1999, where we see that the linear trend for 2,4, and 8-day wavelets curves toward a shallower slope in passing to 16, 32, and 64-day wavelets.

The upward trend of amplitude for image B wavelets at 64 days probably results from the micro-lensing events predicted by the SV 03 model to relate to the luminous quasar Elvis outer structures. Thus we conclude that both the basic time scale found for rapid quasar variability and the linear increase according to the measured structure function seem to favor an origin in an inner band-like M ECO ring with approximately the theoretically expected thickness and radius.

5. Time Scales for Quasar Fueling Events Associated With Unit Mass Ingestion

Fundamental to the understanding of the Quasar luminosity as a response to fueling must be an analysis of time scales associated with the fueling process. We begin with some comments about the nature of mass condensations in the universe.

A fundamental precept of the modern astrophysical view is that the universe is dominated by a non-baryonic "Cold Dark Matter" (CDM) which seeded and developed all structure observed today. We consider the arguments for the existence of this component weak, because the matter has not been found in laboratories despite 15 years of very determined searches, and because observations of the low-redshift (local) universe do not find the expected substructure (Putman and Moore 2002) and because observations at highest redshifts at which galaxies and quasars are observed do not conform to predictions. In particular, at redshifts 4-5, fully assembled galaxies with $10^9 M_{\odot}$ are found far in excess of simulations, and clustering of quasars and galaxies at redshifts 3 - 5 is much stronger than simulated in all CDM simulations. Worse, the high redshift galaxies and quasars are observed to have solar metal abundances, even though the epoch of maximum star formation is expected to be between redshift 1 and 2. And contrary to the CDM theory, dwarf galaxies do not have the cusp-like central structure expected (Spekkens, G iovanelli,

and H aynes, 2005.

The available simulations and theory consistently conclude that on spatial and mass scales relevant for the quasar fueling, structure in the CDM distribution would be unimportant. A possible exception is the report by Diem and, Moore, & Stadel (2005) that CDM clustering on planetary mass scales is observed in simulations for axion Cold Dark Matter.

For the remainder of this report, we adopt the point of view that cold dark matter probably is too diffuse to contribute significantly to the fueling of quasars by discrete mass units. On the other hand, the baryonic dark matter is now known to be significantly aggregated as condensations on specific scales. Stars seem to be in evidence everywhere, and their mass is probably reasonably taken to be in a log-normal distribution with a most probable value of $0.5M_{\odot}$ and a halfwidth of a factor 10 around this most probable value (note that for a log-normal distribution, the mean, mode, and median are not the same, unlike the commonly accepted result for Gaussian statistics). The baryonic dark matter has been identified from quasar micro-lensing as a vast network of "rogue planets" having planetary mass and populating interstellar space everywhere (Schild, 1996, 2004b).

A hydrodynamical theory that predicts this population (Gibson 1996, 1999) as "Primordial Fog Particles" ascribes their origin to fossil fluctuations pervading the universe and forming planetary mass condensations at the time of recombination, 380,000 years after the Big Bang. Since their discovery and interpretation from quasar micro-lensing, they are now being seen in quasar "extreme scattering events" (Walker and Wardle, 1998; Wardle and Walker, 1999) and in "Pulsar Scintillation Scattering" events (Hill et al, 2004). The same hydrodynamical theory that predicts the formation of the "Primordial Fog Particles" (Gibson 1996) also predicts that nature aggregated matter at the time of recombination in globular cluster mass scales, $10^6 M_{\odot}$. These would be the objects mysteriously appearing on short time scales by the thousands during galaxy-galaxy collisions. Nearly all theories of structure formation acknowledge this "Jeans mass" scale of expected structure formation at recombination. This leaves us with a picture of baryonic dark matter having only a small fraction in smoothly distributed gas form, and more importantly aggregated on scales of planets, stars, and globular clusters. Thus we accept these as the unit fueling components for quasars.

The quasar response to this fueling process, seen as brightness fluctuations, has been summarized by De Vries et al (2005, AJ, 129, 615), and summarized as a structure function in their Fig. 8, where we see peaks of heightened brightness variability at time scales of 0.8 years and 9 years (in the quasar rest frame). The 0.8-year feature is particularly well seen in their Fig. 14 for events in their lower luminosity sample (Dark points) at a high

level of significance. We consider that structure function analysis is a poor way to study the 0.8-year fluctuations, and that wavelet analysis, as applied to the Q 0957 brightness statistics by Schild (1999) would be more suitable.

The 9-year events are considered somewhat uncertain by the De Vries et al because of problems combining data sets related to different time scales. The structure function for more rapid variability in the Q 0957 quasar has already been discussed in Section 3. Of course we now seek to match up the De Vries et al (2005) structure function peaks with the fuel units, and we start by associating the 0.8-year (300-day) events with primordial fog particle fueling. De Vries et al (2005) stress that these events are asymmetrical, having typically a slower rise time and more rapid decay, and often but not always accompanied by a color shift toward blue. Typical events of this kind can be seen in the individual brightness curves from Giveon et al, who also reference extensive earlier literature, and Hawkins (1996).

Typical events have amplitude 0.3 mag and time scales (in the quasar rest frame) of approximately 300 days. These typical events have also been seen in the Q 0957 brightness record, where the $(1+z)$ cosmological redshift expands the expected 330-day time scale to approximately 700 days. In the image A (less sensitive to micro-lensing) brightness record shown as Fig. 1 in Pelt et al (1998), three such events are seen peaking at Julian dates $JD - 2440000 = 5800, 7700$, and $10,100$. Observed amplitudes average approximately 0.25 magnitudes. Thus these Q 0957 peaks are typical of unit fueling events seen in all quasars. However, further structure in the Q 0957 brightness history within one of these De Vries et al "events" has been interpreted by SV03 as resulting from internal quasar structure on lags (observer's watch) 125, 190, 540, and 625 days. Thus for Q 0957 the general peak in the De Vries structure function curve includes some component from internal quasar structure.

Since De Vries work implies that high-luminosity quasars vary less than low-luminosity quasars, this result implies a quasar fueling scenario in which: a) variations have a limited absolute magnitude and, b) variations in luminosity are due to unit fueling events involving sub-components or accretion instead of coherent variations of the quasar (De Vries et al (2005)).

In this context we are now in a position to picture the quasar response to a typical unit fueling event. The event has an asymmetrical profile, with a rise time approximately twice as long as the decay time. During the event, the luminous quasar output increased approximately 30 % in UV photons. Since the UV emission is found at nearly the center of the quasar's output spectrum we estimate from this that the quasar total output also increased by approximately 30%.

The average quasar luminosity fluctuation is observed to be on the order of 1×10^{44} ergs/sec, over a 300 day duration. If this luminosity fluctuation is interpreted as being due to the integrated response to a unit planetoid mass ingestion in the disk, then the total integrated energy associated with this process is 3×10^{51} ergs.

Since the unit mass planetoid infall into the quasar accretion disk occurs from large distances, the total energy which contributes to the quasar disk luminosity on impact is equal to its relativistic kinetic energy times an efficiency factor which is estimated to vary between 1 and 10 percent. Since the rest mass energy of a $1 \times 10^{-3} M_{\odot}$ primordial planetoid is comparable to the total integrated energy of the 300 day quasar luminosity fluctuation, this luminosity fluctuation event can be plausibly interpreted as being caused by a collision of the quasar accretion disk with an infalling planetoid with mass on the order of this size which is moving relativistically. In this context the unit fueling process in quasars can be explained energetically in terms of primordial $1 \times 10^{-3} M_{\odot}$ planet-like particles infalling from large distances where the energy conversion to UV luminosity does not need to be very efficient.

This unit quasar fueling mass on the order of $1 \times 10^{-3} M_{\odot}$, is somewhat larger than the $1 \times 10^{-5} M_{\odot}$ unit mass which was previously inferred from quasar micro-lensing considerations Schild (1996). However we do not see this as a contradiction because the micro-lensing process responds to the particles with the largest optical depth, or to the peak of the mass distribution of the micro-lensing particles which is on the order of $1 \times 10^{-5} M_{\odot}$. On the other hand the size of the unit mass ingestion associated with the quasar luminosity fluctuation process will tend to select the more massive $1 \times 10^{-3} M_{\odot}$ particles in the primordial planetoid distribution, since the less massive infalling particles will cause smaller fluctuations not seen in the brightness records.

Since in our scenario the 300-day events found by De Vries et al (2005) and earlier authors are attributable to planetary mass ingestion events, this allows us to make a falsifiable prediction. The structure function analysis presented by De Vries et al is not optimal for studying the nature of the 300-day events because either positive (brightening) or negative (fading) events could be responsible. However our scenario predicts dominant positive events, and a more optimum analysis with wavelets as demonstrated by Schild (1999) would discriminate. Our unit fueling scenario predicts that the 300-day events should be dominated by positive (brightening) wavelets, and wavelet analysis would allow easily interpreted discrimination.

6. Radio Properties of Q 0957 Measured By Micro-lensing

In the following section, we analyze data for Fourier power of the A and B quasar images and conclude that the B image shows more power at micro-lensing frequencies. From this and calculation of the coherence between the radio fluctuations seen, we are able to conclude that the radio emitting region undergoes micro-lensing at radio frequencies. When we estimate the observed amplitude of the measured micro-lensing, we conclude that only a small fraction of the observed radio brightness from the identified region is micro-lensed in the observed "radio microlensing" events.

6.1. The Coherence and Radio Brightness Implied Micro-lensing

Radio emission at 6 cm has been monitored since the 1979 discovery of the Q 0957 quasar by the MIT radio group (Lehar et al, 1992; Haarsma et al 1997, 99). The purpose was to determine the time delay, and one observation per month was made in general. At its high ecliptic latitude, Q 0957 + 561 is far from the sun on any calendar date, and the observing record is of high quality without the annual dropouts characteristic of the optical data.

The basic process is revealed in the Fourier power spectrum for the 6 cm radio emission measured at the VLA. Comparison of the A and B image power spectra shows extremely similar spectra from 0 – 3 cy/yr, which relates to variability on time scales longer than 120 days. But a factor 5 larger power level is seen for image B relative to A between 3 and 5 cycles/yr. Since the radio flux was sampled monthly, the sample frequency is 12 cy/yr and the Nyquist frequency is 6 cy/yr, or 60 days. However, inspection of the brightness record shows the existence of many brightness spikes indicated by 2 or more observations measured with the 30-day basic sampling rate, and thus many individual events having a barely resolved 60-day time scale. Because the B image is seen through the lens galaxy its optical depth to micro-lensing is higher than A. So if a stronger pattern of fluctuations is seen, it is interpreted as arising in micro-lensing. In other words, the A and B image are images of the same quasar, so insofar as their brightness fluctuations differ, we attribute the difference to the micro-lensing that originates in the lens galaxy, and it would be strongest in image B which is seen through the lens galaxy and has a 4 higher optical depth to micro-lensing by the granular structure of matter (stars, planets) in the lens galaxy.

If the higher amplitude of fluctuations limited to 3.5 – 5 cy/yr is caused by micro-lensing, then there must be more spatial structure in the source or more micro-lensing particles of appropriate mass for 3.5 – 5 cycles/yr. The Schild and Vakulik 2003 paper

shows that solar mass micro lenses can produce cusps on this time scale, for the adopted standard transverse velocity of the cusp pattern. However, for micro-lensing to occur, both the fine cusps due to granularity of the mass distribution in the lens galaxy AND fine structure in the radio emission region must be present. This allows us to make size estimates for the radio emitting region. The brightness fluctuations measured as power in Fourier spectral estimates on time scales 3–5 day/yr are best seen in the brightness curves given in Haarsma et al (1999) Fig. 4. We interpret the solid curves in the plot to show the smoothed brightness trend of the two quasar images, and we find many pairs of points that reveal brightness spikes relative to the smoothed trend line. These spikes we interpret as micro-lensing events, and we find that they have typical brightness amplitudes of 5 % on the required time scale, 60 days. Typical events in the B image record are seen at JD – 2440000 = 6600, 7600, 7700, 9400, 9600, and perhaps 10,300. It may also be seen that these events are more commonly seen in the B image than in A, confirming the result of the Fourier power spectrum estimate described above.

Again referring to the SV 03 paper, at optical wavelengths it was estimated from direct simulation that structure on the scale of 2×10^{16} cm produces fluctuations on time scales of 150 days. Thus we conclude from simple scaling arguments that the emitting radio source has a radius of approximately 2.2×10^{16} cm for an adopted mean micro-lensing particle mass of 0.5M (Schild 1996) and for the adopted event duration of 60 days.

6.2. The Micro-lensed Fraction of 6 cm Radio Emission

For structure on such scales, the R/R₀ test of Refsdal & Stabell (1991, 93, 97) cannot be applied because the size of the Einstein ring for a half solar mass star, 2×10^{16} cm, is comparable to the size of the emitting region, as estimated above. Thus the small amplitude of the observed 60-day brightness fluctuations is not indicative of a very large source, but rather is indicative that the micro-lensed source contains only a small fraction of the radio luminosity, as we now estimate.

The amplitude of radio brightness fluctuations has not yet been estimated by wavelet analysis as the optical has (Schild 1999). However we easily estimate the amplitudes of some typical cusp-shaped events from an estimate of the amplitudes of some typical cusp-shaped events from the published radio brightness history, (Haarsma et al 1997, Fig. 4). Here we see that the strongly microlensed B image has typical event amplitudes of 1.4 mJy relative to the mean 25 mJy flux, or approximately 5% microlensing amplitude.

Similarly, the A image has 1.9 mJy amplitude relative to a 35 mJy mean, or 5% amplitude. Because micro-lensing of a very compact source would produce events with amplitudes a factor 10 or 20, we immediately conclude that the radio source component with radius estimate 2.2×10^{16} cm contributes only a small fraction, approximately a percent, of the total measured 6 cm radio brightness.

It is further inferred that the remaining 99% of the measured 6 cm flux originates in a region too large to have micro-lensing events on time scales of 30 days to 10 years, as has been previously inferred. The rapid small brightness fluctuations have sometimes been interpreted in the context of interstellar scintillations (Winn et al, 2004; Koopmans et al, 2003). We consider that the conclusion that over the 3 – 5 cy/yr micro-lensing frequency band, centered at approximately 60 days, the Fourier power measured in the radio brightness curves is higher in the B image than in the A image, in approximately the same ratio as the micro-lensing probability, is a strong indication that the fluctuations originate in micro-lensing. The position of the micro-lensed radio core source along the jet axis is also deduced observationally. The radio and optical brightness has been found to have a substantial coherence with a lag of 35 days, with the optical preceding the radio (Thomson and Schild 1997). Thus apart from geometrical factors, the micro-lensed radio emitting region lies $35 = (1 + z)$ light days above the inner quasar accretion disk structure, or 14.5 light days (3.6×10^{16} cm) above the central source. With correction for the calculated 54 degree inclination of the quasar's rotation axis with respect to the line of sight, the compact micro-lensed radio emitting region is 9×10^{16} cm above the plane of the accretion disc. We conclude that a micro-lensed compact region of radio emission, contributing only a percent of the total radio flux, with a 2×10^{16} cm radius is located 9×10^{16} cm above the accretion disc plane.

6.3. Dynamical Origin of the Micro-Lensed Radio Structure in Q 0957+561 based on MECO Magnetic Field Line Reconnection Processes

Recently the case of radio jet formation from a rotating collapsed object with an intrinsic magnetic dipole field aligned along the rotation axis has been studied (Romano et al, 2004) In that paper it was shown that such a configuration would produce a tangled network of magnetic field lines leading to the creation of magnetic towers associated with vertical quasi-periodic outflows. For the case of the central MECO in the quasar Q 0957+561, we expect that an analogous type of stretching, bunching, breaking, and reconnection of the MECO magnetic field lines should occur at distances comparable to the sizes of the interior quasar SV 03 structure radio structure discussed above.

When such re-connection effects act on the MECO magnetic field lines, the process is likely to entail their breaking and re-connection at the local Alfvén speed. Since the local Alfvén speed will be relativistic in close proximity to the rotating central MECO object, we expect that the field line re-connection process described above has the potential to create the relativistic motions observed in radio jets.

The relativistic Alfvén speed is

$$v_A^2 = \frac{c^2 B^2 = 4}{c^2 + P = (1) + B^2 = 4} \quad (1)$$

In the MECO model in the low hard state, hot plasma containing magnetic field lines is quasi-periodically peeled off the inner magnetospheric radius of the accretion disk in the form of a funnel flow process similar to that described in Romanova et al (2004). In the process of entering the magnetosphere, the poloidal magnetic field components are wound toroidally until $B^2 = 4$ v_A^2 , where $v_k = 0.2c$ is the Keplerian speed of the inner disk.

At the inner disk radius $R = 5 = 3$ and the gas pressure P , which essentially matches the magnetic pressure of the poloidal field component at the edge of the inner disk, is negligible by the time the base of the jet is reached. For this reason, in the toroidally wound donut that falls in through the magnetosphere, the gas pressure P is negligible. The end result of this fact is that the $B^2 = 4 = c^2$ near the base of the jet.

The energy density required for plasma to escape from deep inside the gravitational well is about $GM = r_e$, where r_e is the "ejection radius". At this radius, the energy density of the wound up toroidal magnetic field in the donut is $B^2 = 4$ and this is what drives the jet. Equating these energy densities leads to $r_e = 4 GM = B^2 = GM = v_A^2$. Taking $r_e = 2 \times 10^{16}$ cm from the observed Schild-Vakulik structure, leads to the result that $v_A = 0.16c$, hence the Alfvén speed associated with this process near the MECO is relativistic.

7. Theoretical Analysis and Overview of the Schild-Vakulik Structure (SV 03 structure) Inside of the Quasar Q 0957+361

In this section we discuss the applicability of currently known theoretical quasar models to the empirical Schild-Vakulik Structure (SV 03 structure) discussed in the preceding sections. On the basis of the discussion in the above sections of the paper, that the physical dimensions of the SV 03 structure which exists inside of the quasar Q 0957+361 can be summarized as follows (see figure 1): (IN SETTING UP 1)

Elliptical Emissive Coronal Structure $R_e = 2 \times 10^{17}$ cm, $H_e = 5 \times 10^{16}$ cm

Inner Radius of Accretion Disk $R_m = 74R_g = 3.9 \times 10^{16}$ cm

Size of Hot Inner Accretion Disk Annulus $(R_m) = 1R_g = 5.4 \times 10^{14}$ cm

Size and Location of Base of Radio Structure $R_r = 2 \times 10^{16}$ cm, $H_r = 9 \times 10^{16}$ cm

In the above we note that, since the quasar Q 0957+ 561 has been observed to contain a central compact object with a mass on the order of $M = (3 \text{--} 4) \times 10^9$ solar masses, the observed SV 03 structure inner accretion disk radius of 3.9×10^{16} cm implies that the inner radius of the accretion disk is located at about $74 R_g$. In addition at this radius a hot annulus of material exists with a radial thickness of 5.4×10^{14} cm (which for the above mass is on the order of $1 R_g$ in radial thickness). Finally the hyperbolic Elvis Coronal Structure which is observed in Q 0957+ 561 appears, on the basis of its observed H_r / R_r ratio, to have a rather wide opening angle of 76 degrees with respect to the z-axis of rotation.

At first one might consider explaining the Schild-Vakulik structure (SV 03 structure) in terms of intrinsic magnetic moment generated by a central spinning charged black hole in the quasar Q 0957+ 561. However this explanation fails because the necessary charge on the spinning black hole required to make it work would not be stable enough to account for the long lifetime of the SV 03 structure. This inherent instability occurs because the value of the charge/mass ratios of electrons and protons implies that opposing electric forces on them would then be at least an order of magnitude larger than their gravitational attraction to the central black hole. In addition it would be difficult to maintain this required charge on the spinning black hole if it were also surrounded by an accretion disk like that observed in quasar Q 0957.

Since Q 0957+ 561 appears to be in a radio loud Low Hard State with a very large $74 R_g$ inner accretion disk radius a second attempt to explain the above observations would be to use a standard Kerr Black Hole-ADAF-Accretion Disk-Jet Model (Narayan and Quataert, 2005) One would do this by choosing the parameters in this scenario so that the transition from the hot thin outer disk to the inner ADAF disk occurred at the $74 R_g$ radius. However since the magnetic field in this model is anchored to the accretion disk and not to the central Kerr Black Hole this model cannot account for either: a) the very thin $1 R_g$ radial size of the observed Hot Inner Accretion Disk Annulus at the $74 R_g$ radius or, b) the wide opening Elvis outflow opening angle of 76 degrees with respect to the z-axis of rotation (since the frame dragging on the disk magnetic field that occurs in Kerr Black Hole-ADAF-Accretion Disk-Jet Models characteristically generates jet-like outflows with

relatively narrow opening angles on the order of 30 degrees with respect to the z-axis of rotation, e.g. see figure 1 of the Narayan and Quataert article quoted above).

Since the standard Black Hole-ADAF-Accretion Disk-Jet Model does not predict the SV 03 structure correctly, a third and final attempt to find a black hole description for the SV 03 structure observed in Q 0957+ 561 would be to apply the Magnetically Arrested Disk (MAD) black hole model (Igumenshchev, Narayan, and Abramowicz, 2003), to the above described structure seen in Q 0957+ 561. In this case MAD parameters would be chosen which would set the magnetospheric radius of the MAD accretion disk at $74 R_g$. However in this MAD model description of Q 0957+ 561, instead of the observed hot annular band of material of radial thickness on the order of $1 R_g$, there would now occur at this radius a stochastic injection of hot blobs of plasma which would orbit into the black hole while emitting visible radiation from $74 R_g$ all the way down to the photon orbit at $3 R_g$. Based on the Keplerian orbital periods at these radii, the MAD-black hole model would then generate observable periodic luminosity fluctuations whose local periods at the quasar ranged continuously from 800 days at $74 R_g$ down to 10 days at $R_p = 3 R_g$. Hence if this MAD-Black Hole model had been operating in Q 0957, the clean fluctuation signal associated with the inner hot ring structure of the Schild-Vakulik model would not have been seen because of the smearing out of all of the MAD periodic QPO that would be occurring in the orbital range from $74 R_g$ down to $3 R_g$. Furthermore, periodic brightness fluctuations produced by luminous hot blobs crossing caustics created by the complex mass distribution in lens galaxy G 1 would produce highly periodic, approximately 100-day, brightness spikes not observed.

Hence we find that neither spinning charged black holes, the standard Black Hole-ADAF-Accretion Disk-Jet Model, nor the Black Hole Magnetically Arrested Accretion Disk (MAD) Black hole model, (the latter two of which contain magnetic fields that are assumed to be anchored in the accretion disk and not anchored to the central compact black hole object) can account for all four of the components of SV 03 structure observed within the quasar Q 0957+ 561.

Having tried all of the plausible black hole models and found them unsatisfactory we will now show that the four components of the Schild-Vakulik structure in the quasar Q 0957+ 561 can be consistently described within the context of the Magnetospheric Eternally Collapsing Object (MECO) model, (Robertson and Leiter, 2002, 2003, 2004; Leiter and Robertson, 2003), in which a very strong intrinsic magnetic field, anchored to a slowly rotating highly redshifted central compact MECO object, interacts in a magnetic propeller mode with the surrounding accretion disk and generates the four components of the SV 03 structure with Elvis coronal outflows that can have a wide opening angle greater

that 60 degrees with respect to the z-axis of rotation.

In the following discussion the formal details about the M ECO model which appear in the above papers have been summarized into a series of short appendices (Appendix 1-10) for the convenience of the reader and will be referred to as needed in order to clarify the details of specific calculations. More specific information about the magnetic propeller mode for central compact magnetic objects surrounded by accretion disks can be found in Romano et al. (2002, 2003a).

We begin our M ECO analysis of the SV 03 structure in Q 0957+ 561 starting with Table 1 below in which: a) the left hand column summarizes the M ECO physical quantities relevant to Q 0957+ 561 and the location in the appendixes where for the convenience of the reader the associated derivations and discussions about these physical quantities can be found; b) the middle column gives the specific form of the equations to be used in the calculation of these physical quantities and; c) the right hand column gives the functional form of the relevant mass scaling of these physical quantities in order to demonstrate clearly how the equations for these physical quantities can be applied to the case of both galactic black hole candidates (G B H C) and A G N .

Then, assuming that: a) the M ECO behavior of this quasar in the radio loud Low Hard State is similar to that of an average M ECO -G B H C in the radio loud Low Hard State (like that analyzed in the Robertson-Leiter papers discussed above), and b) using the observed values of: X-ray luminosity, radio luminosity, red shift ($z=1.4$), and the physical dimensions of the internal SV 03 structure for Q 0957+ 561 as input in the mass scaled M ECO equations in Table 1, then c) the results shown in Table 2 are obtained.

Table 2 is intended to be read as follows: in the upper part, the scaling relations from Table 1 and other input data are used to determine the properties of the G B H C and A G N . In the lower panel, the empirical size scale parameters, determined by Schild and Vakulik and corrected for the specific quasar orientation factors in Schild (2005), are scaled and tabulated for the G B H C case according to our adopted scaling relations.

In this manner we found that the presence of a 3.6×10^9 solar mass M ECO acting as the central compact object in the quasar Q 0957+ 561 consistently predicted all of the four components of the observed SV 03 structure. The physical picture which emerged was as follows: 1) since Q 0957 is a radio loud quasar in a LHS then the inner region of the M ECO accretion disk at the magnetospheric radius R_m is larger than the co-rotation radius R_c and the non-thermal M ECO -LHS X-ray emission will be generated by the magnetic propeller interaction of the intrinsic magnetic moment in the central M ECO with the inner accretion disk. 2) The compton scattering force generated within the radiation field environment

around the MECO, acting in conjunction with the MECO intrinsic magnetic propeller interaction with the accretion disc and the magnetic corona about it, then acts to generate the hyperbolic Elvis outflow of plasma 2 10^{17} cm from the central object and with the wide opening angle observed, leading to the development of a radio jet. This structure, has radius R_r given by $2 \cdot 10^{16}$ cm and height H_r of $9 \cdot 10^{16}$ cm. and an Elvis coronal structure of radius $2 \cdot 10^{17}$ cm above and below the inner region of the accretion disk in which the MECO magnetic propeller driven radiation is reprocessed into non-thermal UV and Optical Emissions. 3) The inner region of the accretion disk will be located at $R_m = 1.4 R_c$ where R_m is the magnetospheric radius, and the MECO co-rotation radius R_c is $53 R_g$. A high density, optically thick, radially thin inner band of material of radial thickness given by $0.0135 R_m$ and equal to $5.4 \cdot 10^{14}$ cm is formed by the MECO magnetic propeller at the magnetospheric radius R_m . The thermal emission from this hot optically thick inner band of radial thickness R_m then accounts for the observed small blue thermal bump and its micro-lensing fluctuations. Normalizing the optically thick MECO accretion disk to that of a NS-XRB, we find that the temperature T_t of the thermal emissions from the thin hot inner annulus of material of radial thickness R_m is given by 7191 K. For the observed Q0957 redshift of $z = 1.4$ this thin hot inner annulus generates the observed local thermal "little blue bump" emission wavelength from R_m given by 2697 Angstroms with a thermal UV luminosity L_t equal to $1.4 \cdot 10^{44}$ erg/sec (which is equal to about one quarter of the non-thermal UV luminosity which is generated by Compton up-scattering from the larger hyperbolic Elvis Coronal Structure, also present)

Table 1: MASS SCALING EQUATIONS ASSOCIATED WITH VERY HIGH REDSHIFT EDDINGTON LIMITED MECO - [REF APPENDIX 1-10]

M ECO Physical Quantity	Equation	(M = M ass=M)
Surface Redshift - (App 1, 9-10)	$1 + z_s = 1.5 \cdot 10^8 (M = 7^{1=2})$	M ¹⁼²
Surface Luminosity Obs. - (App 5)	$L_s = L_{Edd} = (1 + z_s) \text{ erg/s}$	M ¹⁼²
Surface Temp Obs. - (App 5)	$T_s = 2.3 \cdot 10^7 = M (1 + z_s)^{1=4} \text{ K}$	M ³⁼⁸
Rotation Rate - (App 7)	$\omega = 0.89 [L_{q;32} = M]^{0.763} = L_{c;36} \text{ Hz}$	M ¹
Quiescent Lum. - (App 7)	$L_{q;32} = 0.65 M [L_{c;36} = M]^{1.75} \text{ erg/s}$	M
Co-rotation Radius - (App 7)	$R_c = 46.7 R_g = M^{2=3} \text{ cm}$	M
Magnetic Radius - (App 7)	$R_m = 3.33 R_g [27 = (L_{Edd}^2 M^{10})]^{1=7} \text{ cm}$	M
Magnetic Moment - (App 7)	$27 = 8.16 [L_{c;36} M = 3^{1=2}] \text{ cm}$	M ⁵⁼²
Magnetic Field - (App 7)	$B = 1.12 (R_g = r)^3 [L_{c;36} = (M^{5/2})]^{1=2} \text{ gauss}$	M ¹⁼²
Radio-X ray Correlation - (App 8)	$L_{rad;36} = 10^{7.11} M^{0.835} L_{x;36}^{2=3} \text{ erg/s}$	M ³⁼²

Table 2: MASS SCALING OF LHS MECO-GBHC TO QUASAR Q 0957

M ECO Physical Quantity	AVG .M ECO-GBHC	M ECO-QUASAR Q 0957
Mass of Central MECO	7 M	3.6 $10^9 M$
Surface Redshift	$1.5 \cdot 10^8$	3.4 10^{12}
Surface Luminosity Obs.	$6.1 \cdot 10^{30} \text{ erg/sec}$	1.4 10^{35} erg/sec
Surface Temp Obs.	$1.3 \cdot 10^5 \text{ K}$	69 K
Rotation Rate	12 Hz	$2.3 \cdot 10^{-8} \text{ Hz}$
Intrinsic Mag. Moment	$2.1 \cdot 10^{30} \text{ gauss-cm}^3$	1.2 $10^{52} \text{ gauss-cm}^3$
Magnetic Field Obs.	$(8.3 \cdot 10^9 \text{ gauss}) (6R_g = r)^3$	$(3.6 \cdot 10^5 \text{ gauss}) (6R_g = r)^3$
Quiescent X-Ray Lum.	$2 \cdot 10^{33} \text{ erg/sec}$	9.4 10^{41} erg/sec
Co-rotation Radius	$53 R_g$	$53 R_g$
X-Ray Lum.	$4.7 \cdot 10^{36} \text{ erg/sec}$	2.4 10^{45} erg/sec
Radio Lum.	$1.1 \cdot 10^{30} \text{ erg/sec}$	1.3 10^{43} erg/sec

Schild-Vakulik Structure	AVG .M ECO-GBHC	M ECO-QUASAR Q 0957
Magnetic Radius	$R_m = 74 R_g = 7.6 \cdot 10^7 \text{ cm}$	$R_m = 74 R_g = 4 \cdot 10^{16} \text{ cm}$
Hot Inner Disk Band	$(R) = R_g = 10^6 \text{ cm}$	$(R) = R_g = 5.4 \cdot 10^4 \text{ cm}$
Base of Radio Jet	$R_r = 5 \cdot 10^7 \text{ cm} H = 2 \cdot 10^8 \text{ cm}$	$R_r = 2 \cdot 10^{16} \text{ cm} H = 9 \cdot 10^{16} \text{ cm}$
Elvis Corona ^a	$R_e = 5 \cdot 10^8 \text{ cm} H = 1.2 \cdot 10^8 \text{ cm}$	$R_e = 2 \cdot 10^{17} \text{ cm} H = 5 \cdot 10^{16} \text{ cm}$

^aElvis Coronal Structure may not be seen in hot LHS MECO-GBHC accretion disks.

Hence in the context of the M ECO model we have shown that the quasar Q 0957+ 561 in a radio loud Low Hard State is physically similar to a mass scaled up version of an average M ECO -G BHC where, because of the cooler accretion disk which occurs in the quasar, all four components of the SV 03 structure are observable. The basic observable elements of the SV 03 structure in this quasar are: 1) a large E lvis elliptical coronal structure with a 76 degree opening angle with respect to the z-axis of rotation; 2) a large magnetospherically generated inner accretion disk radius; 3) a thin hot inner accretion disk annulus located at the magnetospheric radius; and 4) a radio structure whose base is located directly above the central M ECO

We have demonstrated that the M ECO model is able to explain all of the properties of the SV 03 structure observed in the quasar Q 0957+ 561 as intrinsic magnetic propeller interactions with the accretion disk. Hence on this basis we conclude that the presence of the SV 03 structure represents observable evidence for the existence of an intrinsic magnetic moment generated by a central M ECO in the heart of this quasar.

8. Conclusions

We have examined the empirical data for the lensed and micro-lensed Q 0957+561 A,B quasar obtained from 20 years of brightness monitoring at visible wavelengths (near-ultraviolet emission at the quasar). We have also examined several conclusions inferred previously from analysis of the auto-correlation and micro-lensing properties of the monitoring data, and we have now collected these results in a consistent presentation that can confront physical quasar models and their simulations.

The structures and luminosities found, referred to as the Schild-Vakulik structure (SV 03 structure), are associated with a bright inner edge of the accretion disc, surrounded by a coronal outflow (Erlis structure) long known to explain the complex spectroscopic behavior observed in quasars. However it is observed that the opening angle of the coronal Erlis structure with respect to the z-axis of rotation appears to have a very large value of 76 degrees. In addition a radio emission region has been located directly above the compact source. In particular the size and location of this radio emitting region has been found to be located where the reconnection of magnetic field lines at relativistic Alfvén speeds, like that generated by a rotating central object containing an intrinsic magnetic field, should occur.

In the discussion in section 7 we showed that attempts to model observation of the SV 03 structure in the quasar Q 0957+561 in terms of the intrinsic magnetic moment generated by a central spinning charged black hole in the quasar Q 0957+561 failed because the necessary charge on the spinning black hole required to make it work would not be stable enough to account for the long lifetime of the SV 03 structure. Similarly attempts to model the SV 03 structure in terms of the class of Kerr Black Hole-ADAF-Accretion Disc Corona-Jet Models, in which the magnetic field is intrinsic to the accretion disk and not the central rotating black hole, were shown to have difficulty in that they were unable to account for the very large opening angles which are observed for the coronal Erlis outflows. Finally we showed that Magnetically Arrested Disc (MAD) black hole models also have problems in that they predict the existence of orbiting infalling hot blobs of plasma inside of the inner region of the accretion disk that are not observed. In addition these latter two black hole accretion disk models (in which the magnetic field resides in the accretion disk and not in the central compact object) have a problem in that they cannot properly account for the existence of the small radio emitting region which is found to be located directly above the central compact object in the quasar Q 0957+561.

On the other hand we have found that the SV 03 empirical structure can be successfully explained by Magnetospheric Eternally Collapsing Object (M ECO) models, which feature a highly redshifted, Eddington limited, collapsing central compact object containing a strong intrinsic magnetic field aligned with the M ECO axis of rotation. In this model the resultant M ECO magnetic propeller effects which interact with the inner regions of the accretion disc, create an inner luminous annular (band like) structure and an outer coronal structure characterized by strong relativistic outflow with a wide opening angle to the z-axis of rotation as is observed in the SV 03 empirical structure. In particular the size and location of the radio emitting region associated with the SV 03 structure in the quasar Q 0957+ 561 has been found to be located in the region above the central compact object where the reconnection of magnetic field lines at relativistic Alfvén speeds, like that generated by a rotating central M ECO containing an intrinsic magnetic field, should occur.

The M ECO contains a central rotating magnetic object whose dynamo sweeps clean the central region of the quasar out to a distance where the magnetic propeller acts on the inner edge of the accretion disc, and a radio emitting region above the disc where magnetic field lines twist and bunch up until they eventually break and reconnect at relativistic speeds. Such an object does not have an event horizon; instead, in-falling material collects at an inner structure just beyond $2R_g$ that further collapses to higher redshift while remaining in causal connection for all time. Because of the small light cone angle for radiation escaping from this highly redshifted region to the distant observer, the resultant low luminosity in the far-infrared wavelengths make this region difficult to detect in the case of quasar Q 0957+ 561.

It is important to note that the M ECO model that seems to best fit the empirical SV 03 structure in the quasar Q 0957+ 561 differs significantly from most black hole models currently under consideration. In particular the predicted SV 03 empirical structures they generate seem to resemble the complex in-flow-out flow pattern seen in magnetic propeller models for young stellar objects. The action of such magnetic propeller forces has been discussed and simulated by Romanova et al (2003a,b, 2004) with non-relativistic models that produce observable structures that are closely similar to the observed Schild-Vakulik structure.

We have also found that the M ECO explanation of the empirical SV 03 structure implies an interesting similarity between the M ECO model for the quasar Q 0957+ 561 and the M ECO models that explain the phenomena associated with Galactic Black Hole Candidates in the Low Hard state with luminosity on the order of one tenth of a percent of the Eddington limit luminosity.

On the basis of the above observational and theoretical arguments we conclude that

the observation of the Schild-Vakulik structure in the quasar Q 0957+ 561 represents strong evidence for the existence of an observable intrinsic magnetic moment, generated by a supermassive $3.6 \times 10^9 M_{\odot}$ MECO acting as the central compact object in this active galaxy, which implies that this quasar does not have an event horizon.

9. Appendix 1 - Magnetospheric Eternally Collapsing Objects (MECO)

Using the Einstein-Maxwell Equations and Quantum Electrodynamics in the context of General Relativistic plasma astrophysics we have found that it is possible to virtually stop and maintain a slow, (in any Hubble times!) steady collapse of a compact physical plasma object outside of its Schwarzschild radius with photon pressure generated by synchrotron radiation from an equipartition surface magnetic field. To control the rate of collapse, the object must radiate at the local Eddington limit, but from a highly redshifted surface.

In Appendix 9 and 10, we show that surface drift currents within a pair plasma at the MECO surface generate its required fields. Drift currents proportional to $g \cdot B = B^2$ occur for plasma at rest in gravitational and magnetic fields. The equatorial poloidal magnetic field associated with a stable rate of collapse of the exterior surface is 10^{20} gauss. Fields of this magnitude are strong enough to create electron-positron pairs out of the quantum electrodynamic vacuum. This assures sufficient photon pressure from annihilation radiation to stabilize the collapse rate. The magnetic field of the interior is approximately what one would expect from flux compression during collapse, $2.5 \times 10^{13} \frac{q}{7M} M_{\odot}$ gauss and its radial component is continuous across the surface boundary. The poloidal field is discontinuous across the surface and much stronger externally due to the surface drift currents. As shown in Appendix 10, at the MECO surface radius R_s (which is slightly larger than the Schwarzschild radius $2GM = c^2$), the ratio of poloidal field on the surface to the poloidal field just under the MECO surface is given by

$$B_{s^+} = B_{s^-} = (1 + z_s) = (2 \ln(1 + z_s)) = 10^{20} = (2.5 \times 10^{13}) \frac{q}{7M} M_{\odot} \quad (2)$$

where z_s is the surface redshift. This has the solution

$$1 + z_s = 1.5 \times 10^8 \frac{q}{M} M_{\odot} \quad (3)$$

The distantly observed field is reduced by a surface redshift of by a factor of $3(1 + z_s) = 4.5 \times 10^8 \frac{q}{M} M_{\odot}$ to a level which agrees well with the observed GBC magnetic moments. The surface luminosity is reduced below the conventional Newtonian Eddington limit by $(1 + z_s)$ when distantly observed, and the decay lifetime is extended by the same factor. Figure 2 represents a schematic diagram summarizing the physical mechanisms contributing to the creation of a MECO in the general relativistic gravitational collapse process, which are discussed in the following appendix sections of this paper. (INSERT FIGURE 2)

10. Appendix 2 – The Strong Principle of Equivalence

Astrophysicists now days generally accept the inevitability of the curvature singularities of black holes⁴, however, if GR and AGN are observationally confirmed as containing intrinsic magnetic moments, this will be nature's way of telling us that such singularities are not really permitted to exist. For black holes to exist, gravity must be able to do what no other force of nature can do; namely, to accelerate finite mass to exactly the speed of light. But this means that horizon crossing geodesics would become null rather than timelike. In General Relativity (GR) the Strong Principle of Equivalence (SPE) requires that Special Relativity (SR) must hold locally for all time-like observers in all of spacetime. This SPE requirement is a tensor relationship that implies that (i) the spacetime manifold for observers located in field-free regions, distant from gravitating masses, must approach the flat spacetime of SR⁵ and (ii) the spacetime world lines of massive matter must always be timelike.⁶ Such spacetime manifolds are known as 'bundle complete' [Wheeler & Ciufolini 1995] As a guiding principle, we look for solutions of the Einstein equations

$$G_{\mu\nu} = (8\pi G/c^4)T_{\mu\nu} \quad (4)$$

that satisfy the SPE requirement for timelike world line completeness. Since there is nothing in the Einstein tensor $G_{\mu\nu}$ that enforces this condition, we must rely on non-gravitational

⁴The modern notion of a black hole began with Hilbert's error of application of boundary conditions for the solutions of Einstein's field equations of General Relativity for a mass point. Hilbert's solution has been erroneously attributed to Schwarzschild, however Schwarzschild's preceding original solution had no event horizon. [see Abrams 1979, 1989] Nevertheless, Hilbert's solution is analytically extendible through the horizon to a central singularity, hence the modern black hole. The fact that the radius of the event horizon, which is directly proportional to the gravitational mass, can be changed arbitrarily by (generally singular) coordinate transformation strongly suggests that the horizon is unphysical.

⁵This eliminates Kruskal-Szekeres coordinates from the real world of astrophysics.

⁶Models of gravitational collapse that lead to the development of event horizons and central curvature singularities inevitably abandon the SPE requirement for timelike world line completeness. The vanishing of the metric time coefficient, g_{tt} , at the Schwarzschild radius is sufficient to cause free-fall geodesics of test particles in non-singular Finkelstein or Kerr-Schild coordinates, for constant central mass, to become null at the event horizon. In either coordinates, the crossing can be accomplished in a finite proper time because the proper time stops on a null geodesic. More surprisingly, it also requires only a finite coordinate time for Kerr-Schild. It has been shown [Leiter & Robertson 2003] that null geodesics occur at surfaces of infinite redshift. In Kruskal-Szekeres coordinates, in which g_{tt} does not vanish, there is no surface of infinite redshift at the Schwarzschild radius, $R = 2GM/c^2$, and timelike test particle geodesics can traverse it in either direction, so long as the initial conditions are chosen in a manner that permits the 'time' coordinate to change in a positive sense. However, a central singularity still exists in these coordinates and they have a surface of infinite redshift as $r \rightarrow 1$, at which outgoing geodesics become null. This is an extreme example of a coordinate transformation changing the size of the event horizon radius.

forces in T to dynamically enforce it. Since the energy-momentum tensor T serves as both a source of curvature in the Einstein equations and a generator of the equations of motion of matter, constraints on T that enforce timelike world line completeness can also eliminate the occurrence of event horizons. Thus the SPE requires that the right hand side of the GR field equation must contain non-gravitational elements capable of stopping the collapse of physical matter before the formation of a 'trapped surface'. This dynamically escapes the Hawking and Penrose theorem which states that once a trapped surface is formed, an event horizon and curvature singularities are unavoidable.

In what follows we will show how the SPE constrains the solutions of the Einstein field equations. Consider a comoving interior metric given by

$$ds^2 = A(r; t)^2 c^2 dt^2 - B(r; t)^2 dr^2 - R(r; t)^2 (d^2 + \sin^2 d^2) \quad (5)$$

and an exterior Vaidya metric with outgoing radiation

$$ds^2 = (1 - 2GM/c^2R)c^2 du^2 + 2cdudR - R^2(d^2 + \sin^2 d^2) \quad (6)$$

where R is the areal radius and $u = t - R/c$ is the retarded observer time. Following Lindquist, Schwarz & Misner [1965], we define

$$= \frac{dR}{dl} \quad (7)$$

$$U = \frac{dR}{d} \quad (8)$$

$$M(r; t) = 4 \int_0^r R^2 \frac{dR}{dr} dr \quad (9)$$

$$= \left(\frac{dR}{dl} \right)^2 = 1 - \frac{2GM(r; t)}{c^2R} + \frac{U^2}{c^2} \quad (10)$$

where dl is a proper length element in a zero angular momentum comoving frame, d an increment of proper time, U is the proper time rate of change of the radius associated with the invariant circumference of the collapsing mass, and $M(r; t)$ is the mass enclosed within this radius. The last two of the relations above have been obtained from the G_0^0 component of the field equation [Lindquist, Schwarz & Misner 1965]. At the boundary of the collapsing, radiating surface, s , we find that the proper time will be positive definite, as required for timelike world line completeness if

$$d_s = \frac{du}{1 + z_s} = du \left((1 - \frac{2GM(r; t)_s}{c^2R_s})^{1/2} + \frac{U_s^2}{c^2} \right)^{1/2} > 0 \quad (11)$$

where z_s is the distantly observed redshift of the collapsing surface. From the above equation we see that in order to avoid a violation of the requirement of timelike world line

completeness for $U_s < 0$, it is necessary to dynamically enforce the 'no trapped surface condition'.⁷

$$\frac{2GM_s}{c^2R_s} < 1 \quad (12)$$

11. Appendix 3 - A Radiating, Collapsing, Magnetic Object

The simplest form of the energy-momentum tensor that can satisfy the SPE requirement of time-like world line completeness, is one that describes a collapsing, radiating plasma with an equipartition magnetic field that emits its outgoing radiation. Between the extremes of pure magnetic energy [Thorne 1965] and weakly magnetic, radiation dominated polytropic gases or pressureless dust [Baumgarte & Shapiro 2003] there are cases where the rate of collapse can be stable. To first order, in an Eddington limited radiation dominated context, these can be described by the energy-momentum tensor:

$$T = (+ P = c^2)u u - P + E \quad (13)$$

where $E = Q k k$, $k k = 0$ describes outgoing radiation in a geometric optics approximation, Q is energy density of matter and P the pressure.⁸ Here Q is given by

$$Q = \frac{(dM_s = du) = 4 \pi R^2}{(c_s + U_s = c)^2} \quad (14)$$

At the comoving MECO surface the luminosity is

$$L = 4 \pi R^2 Q > 0: \quad (15)$$

and the distantly observed luminosity is

$$L_1 = c^2 \frac{dM_s}{du} = c^2 \frac{dM_s}{d(1 + z_s)} \quad (16)$$

⁷ It might be argued that there might not be a surface that physically divides matter from radiation inside a collapsing massive continuum, however, it has been shown [Mitra 2000, 2002, Leiter & Robertson 2003] that the above equations and the G_0^0 field equation in a zero angular momentum comoving frame produces the 'no trapped surface condition' for any interior $R(r,t)$, provided that $B(r,t)$ does not become singular at a location where $A(r,t)$ vanishes. However this requirement will be satisfied as long as timelike world line completeness is maintained by photon pressure generated by the equipartition magnetic field everywhere in the comoving frame. We can consider any interior location and the radiation flux there without requiring a pinched Vaidya metric. But there will ultimately be an outer radiating boundary and the required match to the non-singular outgoing exterior Vaidya metric guarantees that there will be no metric singularity there.

⁸ Energy-momentum tensors corresponding to metrics describing ingoing radiation, which are used in many black hole model calculations, (e.g. Baumgarte & Shapiro [2003]) cannot be used here because they are incompatible with the $Q > 0$ boundary conditions associated with collapsing, outwardly radiating objects.

After examining the relations between surface and distantly observed luminosities, we will use this relation to determine the MECO lifetime.

12. Appendix 4 - Eddington limited MECO

Among the various equations associated with the collapse process there are three proper time differential equations applicable to a compact collapsing and radiating physical surface. When evaluated on the physical surface [Hernandez Jr. & Misner, 1966, Lindquist, Schwartz & Misner 1965, Misner 1965, Lindquist, 1966] these equations are:

$$\frac{dU_s}{d} = \left(\frac{2}{1 + P = c^2} \right)_s \left(\frac{\partial P}{\partial R} \right)_s \left(\frac{GM + 4R^3(P + Q) = c^2}{R^2} \right)_s \quad (17)$$

$$\frac{dM_s}{d} = \left(4R^2P \frac{U}{c} \right)_s \left(L \left(\frac{U}{c} + \right) \right)_s \quad (18)$$

$$\frac{dL_s}{d} = \frac{G}{c^4} \left(\frac{L}{R} \right)_s + \frac{U_s}{c^2} \left(\frac{2}{1 + P = c^2} \right)_s \left(\frac{\partial P}{\partial R} \right)_s \quad (19)$$

In Eddington limited steady collapse, the conditions $dU_s/d = 0$ and $U_s = 0$ hold after some time, t_{Edd} , that has elapsed in reaching the Eddington limited state. Then

$$\frac{dU_s}{d} = \frac{2}{(1 + P = c^2)_s} \left(\frac{\partial P}{\partial R} \right)_s \left(\frac{GM_s}{R_s^2} \right) = 0 \quad (20)$$

where

$$M_s = (M + 4R^3(P + Q) = c^2)_s \quad (21)$$

includes the magnetic field energy in the pressure term and radiant energy in Q . Eq. (19) when integrated over a closed surface can be solved for the net outward flow of Eddington limited luminosity through the surface. Taking the escape cone factor of $27(R_g = R_s)^2 = (1 + z_s)^2$ into account, where $R_g = GM = c^2$, the outgoing (but not all escaping) surface luminosity, L , would be

$$L_{\text{Edd}} (\text{outflow})_s = \frac{4GM_s c R^2 (1 + z_{\text{Edd}})^3}{27 R_g^2} \quad (22)$$

where $0.4 \text{ cm}^{-2} = g$ is the plasma opacity. (For simplicity, we have assumed here that the luminosity actually escapes from the MECO surface rather than after conveyance through a MECO atmosphere and photosphere. The end result is the same for distant observers.) However the luminosity L_s which appears in the above equations is actually the net luminosity, which escapes through the photon sphere, and is given by $L_s = L_{\text{Edd}} (\text{escape})_s =$

$L_{Edd}(\text{outflow}) - L_{Edd}(\text{fallback}) = L_{Edd;s} - L_{Edd;s}(1 - 27R_g^2) = (R(1 + z_{Edd}))^2$ Thus in Eqs (17) and (18), the L_s appearing there is given by

$$L_s = L_{Edd}(\text{escape})_s = \frac{4 \pi G M_s (1 + z_{Edd})}{c^2} \quad (23)$$

In this context from Eqs (9), (10), (17) and (22) we have

$$c^2 \frac{dM_s}{d} = \frac{L_{Edd}(\text{escape})_s}{(1 + z_s)} = \frac{4 \pi G M_s (1 + z_s)}{c^2} \quad (24)$$

which can be integrated to give

$$M_s(\tau) = M_s(\tau_{Edd}) \exp((4 \pi G/c^2) \tau_{Edd}) \quad (25)$$

This yield a distantly observed MECO lifetime of $(1 + z_s) \approx 4 \pi G/c^2 \approx 5 \times 10^{16} \text{ yr}$ for $z_s = 10^8$. Finally, equation (18) becomes

$$\frac{dM_s}{d} = \frac{G}{c^4} \frac{L_{Edd;s}}{R_s(\tau_{Edd})} \quad (26)$$

which, in view of (13) has the solution

$$M_s(\tau) = \frac{1}{1 + z_s(\tau)} = (1 - \frac{2GM_s(\tau_{Edd})}{c^2 R_s(\tau_{Edd})})^{1/2} > 0 \quad (27)$$

which is consistent with Eqs (9) and (11). If one naively attributes Eddington luminosity to purely thermal processes, one quickly finds that the required MECO surface temperatures would be so high that photon energies would be far beyond the pair production threshold and the compactness would assure that photon-photon collisions would produce numerous electron-positron pairs. Thus the MECO surface region must be dominated by a pair plasma. Pelletier & Maccarone [1998] have shown that the energy density of magnetic perturbations in equipartition pair plasma is preferentially converted to photon pressure, rather than causing particle acceleration. The radiative power of an equipartition pair plasma is proportional to B^4 , (pair density / B^2 and synchrotron energy production / B^2 .) Lacking the equipartition pair plasma, magnetic stress, $B^2 = 8$, and gravitational stress, $G M_s = R_s$, would both increase as R_s^{-4} during gravitational collapse. Magnetic fields much below equipartition levels would be incapable of stopping the collapse. However, since photon pressure generated by the pairs at equipartition increases more rapidly than gravitational stresses, it is possible to stabilize the rate of collapse at an Eddington luminosity rate. With this extremely efficient photon-photon pair production mechanism, the radiation temperature and pressure is buffered near the pair production threshold by two types of highly redshifted quantum electrodynamic phase transitions which convert photons into pairs on the MECO surface. The first one involves optically thick

photon-photon pair production while the second one occurs for MECO surface magnetic fields strong enough to create bound pairs out of the quantum electrodynamic vacuum. In the context of an Eddington limited balance generated by the former process, the latter process can lead to excess production of pairs, followed by excess photon pressure and an expansion of the MECO surface. In this manner the MECO Eddington limited collapse rate is inherently stable (see Appendix 9 and 10). Stability is maintained by increased (decreased) photon pressure ($\propto B^4$) if the field is increased (decreased) by compression or expansion. For equipartition conditions, the field also exceeds that required to confine the pair plasma. Since the photon luminosity is not confined to the core it will not be trapped, as occurs with neutrinos, however, the radiation should be thermalized as it diffuses through an optically thick environment. To reduce the field to the distantly observed levels implied by our analysis of GBHC and AGN observations would require the existence of a redshift of $z = 1.5 \times 10^8 (M = 7M_\odot)^{1/2}$ (see Appendixes 9 and 10). The residual, distantly observable magnetic moment and extremely faint, redshifted radiations would be the only things that would distinguish such an object from a black hole.⁹

An electron-positron pair atmosphere of a MECO is an extremely significant structure that conveys radiation from the MECO surface to a zone with a much lower redshift and larger escape cone from which it escapes. In order to describe this process computationally within a numerical grid, a radial grid interval no larger than $10^{-8} R_g$ would be needed, where $R_g = GM/c^2$ is the gravitational radius. Although there have been many numerical studies of the behavior of collapsing compact objects in GR, to our knowledge none have sufficient numerical resolution to examine the extreme redshift regime associated with MECO nor have they considered the emergent properties of equipartition magnetic fields and pair plasma at high redshift. Until computer models of gravitational collapse encompass these crucial physical and computational elements, simulations that apparently

⁹An additional point of support for very large values of redshift concerns neutrino transport in stellar core collapse. If a diffusion limited neutrino luminosity of 10^{52} erg/s [Shapiro & Teukolsky 1983] were capable of very briefly sustaining a neutrino Eddington limited rate of collapse, then the subsequent reduction of neutrino luminosity as neutrino emissions are depleted and trapped in the core would lead to an adiabatic collapse, magnetic flux compression, and photon emissions reaching an Eddington limit. At this point the photon luminosity would need to support a smaller diameter and more tightly gravitationally bound mass. A new photon Eddington balance would thus require an escaping luminosity reduced by at least the 10^{20} opacity ratio ($\tau = \sigma_T / \sigma_N$), where $\sigma_T = 6.6 \times 10^{-25} \text{ cm}^2$ is the Thomson cross section and $\sigma_N = 4.4 \times 10^{-45} \text{ cm}^2$ is the neutrino scattering cross-section. Thus $L_1 < 10^{31} \text{ erg/s}$ would be required. For this to correspond to an Eddington limit luminosity as distantly observed would require $1 + z = 10^8$. The adiabatic relaxation of neutrino support and formation of a pair plasma is an important step in gravitational collapse that is not encompassed by polytropic equation of state models of collapse. It is of some interest that if neutrinos have non-zero rest mass they might be trapped inside the photon sphere anyway.

produce black hole states must be regarded as mere scientific nonsense.

13. Appendix 5 - The Quiescent MECO

The quiescent luminosity of a MECO originates deep within its photon sphere. When distantly observed it is diminished by both gravitational red shift and a narrow exit cone. The gravitational red shift reduces the surface luminosity by $1/(1+z)^2$ while the exit cone further reduces the luminosity by the factor $27R_g^2/(R(1+z))^2 = 27/(4(1+z)^2)$ for large z . Here we have used

$$\frac{R_g}{R} = \frac{1}{2} \left(1 - \frac{1}{(1+z)^2}\right) < \frac{1}{2} \quad (28)$$

where R and z refer to the location from which photons escape. The net outflow fraction of the luminosity provides the support for the collapsing matter, thereby dynamically maintaining the EEP requirement of timelike world line completeness. The photons which finally escape do so from the photosphere of the pair atmosphere. The fraction of luminosity from the MECO surface that escapes to infinity in Eddington balance is

$$(L_{Edd})_s = \frac{4 \pi G M_s c (1+z)}{R^2} = 1.27 \times 10^{38} m (1+z_s) \text{ erg/s} \quad (29)$$

where $m = M = M_{\odot}$. The distantly observed luminosity is:

$$L_1 = \frac{(L_{Edd})_s}{(1+z_s)^2} = \frac{4 \pi G M_s c}{(1+z_s)^3} \quad (30)$$

When radiation reaches the photosphere, where the temperature is T_p , the fraction that escapes to be distantly observed is:

$$L_1 = \frac{4 \pi R_g^2 T_p^4 27}{(1+z_p)^4} = 1.56 \times 10^7 m^2 T_p^4 \frac{27}{(1+z_p)^4} \text{ erg/s} \quad (31)$$

where $\sigma = 5.67 \times 10^{-5} \text{ erg/s/cm}^2$ and subscript p refers to conditions at the photosphere. The above equations yield:

$$T_1 = T_p = (1+z_p) = \frac{2.3 \times 10^7}{(m (1+z_s))^{1/4}} \text{ K} : \quad (32)$$

To examine typical cases, a $10M_{\odot}$, $m = 10$ GBC modeled in terms of a MECO with $z = 1.5 \times 10^8$ ($m = 7$) $^{1/2}$ would have $T_1 = 1.1 \times 10^5 \text{ K} = 0.01 \text{ keV}$, a bolometric luminosity, excluding spin-down contributions, of $L_1 = 7.3 \times 10^{30} \text{ erg/s}$, and a spectral peak at 220 \AA^0 , in the photoelectrically absorbed deep UV. For an $m = 10^7$ AGN, $T_1 = 630 \text{ K}$,

$L_1 = 7.2 \times 10^{33}$ erg=s and a spectral peak in the infrared at 4 . (Sgr A at $m = 3 \times 10^6$, would have $T_1 = 1100$ K, and a 2.2 m micron brightness below 0.6 m Jy; more than an order of magnitude below the observational upper limit of 9 m Jy [Reid et al. 2003].) Hence passive MECO without active accretion disks, although not black holes, have lifetimes much greater than a Hubble time and emit highly redshifted quiescent thermal spectra that may be quite difficult to observe. There are additional power law components of similar magnitude that originate as magnetic dipole spin-down radiation. Escaping radiation passes through a pair plasma atmosphere that can be shown, ex post facto to be radiation dominated throughout. Under these circumstances, the radiation pressure within the equilibrium atmosphere obeys $P_{rad} = (1 + z) = \text{constant}$.¹⁰ Thus the relation between surface and photosphere temperatures is $T_s^4 = (1 + z_s) = T_p^4 = (1 + z_p)$. At the MECO surface, we expect a pair plasma temperature of $T_s = m_e c^2 = k = 6 \times 10^9$ K because an equipartition magnetic field effectively acts as a thermostat which buffers the temperature of the optically thick synchrotron radiation escaping from the MECO surface [Pelletier & Marcowith 1998]. But since $T_1 = T_p = (1 + z_p)$, and using $T_s = 6 \times 10^9$ K, we have that

$$T_p = T_s \left(\frac{T_s}{T_1 (1 + z_s)} \right)^{1/3} = 3.8 \times 10^{10} \frac{m^{1/12}}{(1 + z_s)^{1/4}} = 4.5 \times 10^8 (m = 7)^{1/24} \text{ K} \quad (33)$$

In the last expression, we have used $1 + z_s = 1.5 \times 10^8 (m = 7)^{1/2}$. Using the above equations, this leads immediately to $(1 + z_p) = 3500 (m = 7)^{1/3}$, independent of the surface redshift, thus confirming that for MECO with pair atmospheres to exist, they must be inherently highly redshifted. Due to the very weak dependence of T_p on m , the photosphere temperatures of MECO are all very nearly 4.5×10^8 K.

14. Appendix 6 – An Accretively Accreting MECO

From the viewpoint of a distant observer, accretion would deliver mass-energy to the MECO, which would then radiate most of it away. The contribution from the central MECO alone would be

$$L_1 = \frac{4 \pi M_s c}{(1 + z_s)} + \frac{m_1 c^2}{1 + z_s} (e(1 + z_s) - 1) = 4 \pi R_g^2 T_p^4 \frac{27}{(1 + z_p)^4} \quad (34)$$

¹⁰Due to its negligible mass, we consider the pair atmosphere to exist external to the MECO. Due to the slow collapse, the exterior Vaidya metric can be approximated by exterior, outgoing Finkelstein coordinates. In this case, the hydrostatic balance equation within the MECO atmosphere is $\frac{\partial p}{\partial r} = -\frac{\partial \ln(g_{00})}{2\partial r} (p + c^2)$, where $g_{00} = (1 - 2R_g/r)$ and $c^2 \ll p$. This integrates to $p = (1 + z) = \text{constant}$.

where $e = E/m c^2 = 0.943$ is the specific energy per particle available after accretion disk flow to the marginally stable orbit radius, r_{ms} . Assuming that m_1 is some fraction, f , of the Newtonian Eddington limit mass accretion rate, $4 \pi G M c =$, then

$$1.27 \cdot 10^{38} \frac{m}{1 + z_s} = (27) (1.56 \cdot 10^7) m^2 \left(\frac{T_p}{1 + z_p} \right)^4 \quad (35)$$

where $= 1 + f((1 + z_s)e - 1)$ includes both quiescent and accretion contributions to the luminosity. Due to the extremely strong dependence on temperature of the density of pairs, (see Appendix 9 and 10) it is unlikely that the temperature of the photosphere will be greatly different from the average of $4.6 \cdot 10^8 K$ found previously for a typical GBHC. Assuming this to be the case, along with $z = 10^8$, $m = 10$, and $f = 1$, we find $T_1 = T_p = (1 + z_p) = 1.3 \cdot 10^7 K$ and $(1 + z_p) = 35$, which indicates considerable photospheric expansion. The MECO luminosity would be approximately Newtonian Eddington limit at $L_1 = 1.2 \cdot 10^{39} \text{ erg/s}$. For comparison, the accretion disk outside the marginally stable orbit at r_{ms} (efficiency = 0.057) would produce only $6.8 \cdot 10^{37} \text{ erg/s}$. Thus the high accretion state luminosity of a GBHC would originate primarily from the central MECO. The thermal component would be 'ultrasoft' with a temperature of only $1.3 \cdot 10^7 K$ (1.1 keV). A substantial fraction of the softer thermal luminosity would be Compton scattered to higher energy in the plunging flow inside r_{ms} . Even if a disk flow could be maintained all the way to the MECO surface, where a hot equatorial band might result, the escaping radiation would be spread over the larger area of the photosphere due to photons origins deep inside the photon orbit.

For radiation passing through the photosphere most photons would depart with some azimuthal momentum on spiral trajectories that would eventually take them across and through the accretion disk. Thus a very large fraction of the soft photons would be subject to bulk Comptonization in the plunging region inside r_{ms} . This contrasts sharply with the situation for neutron stars where there probably is no comparable plunging region and few photons from the surface cross the disk. This could account for the fact that hard x-ray spectral tails are comparatively much stronger for high state GBHC. Our preliminary calculations for photon trajectories randomly directed upon leaving the photon sphere indicate that this process would produce a power law component with photon index greater than 2. These are difficult, but important calculations for which the effects of multiple scattering must be considered. But they are beyond the scope of this paper, which is intended as a first description of the general MECO model.

15. Appendix 7 - Magnetosphere - Disk Interaction

In LM XB, when the inner disk engages the magnetosphere, the inner disk temperature is generally high enough to produce a very diamagnetic plasma. This may not be the case for AGN. Surface currents on the inner disk distort the magnetopause and they also substantially shield the outer disk such that the region of strong disk-magnetosphere interaction is mostly confined to a ring or torus, of width r and half height H . This shielding leaves most of the disk under the influence of its own internal shear dynamo fields, [e.g. Balbus & Hawley 1998, Balbus 2003]. At the inner disk radius the magnetic field of the central MECO is much stronger than the shear dynamo field generated within the inner accretion disk. In MHD approximation, the force density on the inner ring is $F_v = (r \cdot B) \cdot B = 4$. For simplicity, we assume coincident magnetic and spin axes of the central object and take this axis as the z axis of cylindrical coordinates $(r; \theta; z)$. The magnetic torque per unit volume of plasma in the inner ring of the disk that is threaded by the intrinsic magnetic field of the central object, can be approximated by $v = rF_v = r \frac{B_z \partial B}{4 \partial z} = r \frac{B_z B}{4 H}$, where B_z is the average azimuthal magnetic field component. We stress that B_z , as used here, is an average toroidal magnetic field component. The toroidal component likely varies episodically between reconnection events [Goodson & Winglee 1999, Matt et al. 2002, Kato, Hayashi & Matsumoto 2004, Uzdensky 2002]. The average flow of disk angular momentum entering the inner ring is $M_{-}rv_k$, where M_{-} is mass accretion rate and v_k is the Keplerian speed in the disk. This angular momentum must be extracted by the magnetic torque, hence:

$$= M_{-}rv_k = r \frac{B_z B}{4 H} (4 rH - r) : \quad (36)$$

In order to proceed further, we assume that $B_z = B_z$, $B_z = r^3$, and use $v_k = \frac{GM}{r^2}$, where q is a constant, presumed to be of order unity, q is the magnetic dipole moment of the central object M , its mass, and G , the Newtonian gravitational force constant. With these assumptions we obtain

$$M_{-} = \left(\frac{r}{r_m} \right) \frac{r^2}{r^5 v_k} \quad (37)$$

where $v_k = r$ and the magnetopause radius, r_m is given by

$$r_m = \left(\frac{r}{r_m} \right)^{2/7} \left(\frac{4}{GM M^{-2}} \right)^{1/7} \quad (38)$$

In order to estimate the size of the boundary region, ($r=r_m$), we normalized this disk-magnetosphere model for agreement with radii calculated for an elaborate model of a gas pressure dominated disk [Ghosh & Lamb 1992]. Although we find the portion of the

inner disk threaded by magnetic fields to be smaller than the G hosh & Lamb model, this size for the inner radius yields very accurate results for accreting millisecond pulsars, which have known magnetic moments. We find $(\frac{r}{r}) = 0.015$. Using units of 10^{27} gauss cm³ for magnetic moments, 100 Hz for spin, 10^6 cm for radii, 10^{15} g/s for accretion rates, solar mass units, $r=r=0.015$ and otherwise obvious notation, we find the magnetosphere radius to be:

$$r_m = 4 \times 10^6 \left(\frac{4}{m \cdot 0.015} \right)^{1/7} \text{ cm} \quad (39)$$

where $m = M = M_\odot$ and the disk luminosity is

$$L = \frac{GMm}{2r_m} \quad (40)$$

The co-rotation radius, at which disk Keplerian and magnetosphere spins match is:

$$r_c = 7 \times 10^6 \left(\frac{m}{2} \right)^{1/3} \text{ cm} \quad (41)$$

The low state disk luminosity at the co-rotation radius is the maximum luminosity of the true low state and is given by:

$$L_c = \frac{GMm}{2r_c} = 1.5 \times 10^{34} \left(\frac{2}{27} \right)^{2/3} m^{-1} \text{ erg/s} \quad (42)$$

The minimum high state luminosity for all accreting matter being able to reach the central object occurs at approximately the same accretion rate as for L_c and is given by:

$$L_{\text{min}} = \eta \dot{m} c = 1.4 \times 10^{36} \left(\frac{2}{27} \right)^{7/3} m^{5/3} \text{ erg/s} \quad (43)$$

Where $\eta = 0.42$ for MECO for the photon sphere¹¹ and $\eta = 0.14$ for NS is the efficiency of accretion to the central surface.

For a MECO in true quiescence, the inner disk radius is larger than the light cylinder radius. In NS, and GBC and AGN modeled as MECO, the inner disk may be ablated due to radiation from the central object. The inner disk radius can be ablated to distances larger than 5×10^4 km because optically thick material can be heated to 5000K and ionized by the radiation. The maximum disk luminosity of the true quiescent state occurs with the inner disk radius at the light cylinder, $r_{lc} = c = r_m$. The maximum luminosity of the quiescent state is typically a factor of a few larger than the average observed quiescent luminosity.

$$L_{\text{max}} = (2.7 \times 10^{30} \text{ erg/s}) \left(\frac{2}{27} \right)^{9/2} m^{1/2} \quad (44)$$

¹¹The time for a luminosity variation to be observed is very long for energy released by processes inside the photon sphere.

We calculate the average quiescent luminosities in the soft x-ray band from 0.5–10 keV using the correlations of Possenti et al. [2002] with spin-down energy loss rate as:

$$L_q = E = 4^2 I \quad (45)$$

where I is the moment of inertia of the star, E its rate of spin and a multiplier that can be determined from this new $E - L_q$ correlation for given E ; i.e., known spin and magnetic moment. In previous work we had used $= 10^3$ for all objects, but $3 \cdot 10^4$ would be the average value, for G B H C and AGN modeled as M ECO, consistent with the Possenti correlation. We assume that the luminosity is that of a spinning magnetic dipole for which $E = 32^4 I^2 / 3c^3$, (Bhattacharya & Srinivasan 1995) where I is the magnetic moment. Thus the quiescent x-ray luminosity would then be given by:

$$L_q = \frac{32^4 I^2}{3c^3} = 3.8 \cdot 10^{33} \cdot \frac{I^2}{27^2} \text{ erg/s} \quad (46)$$

According to the Possenti correlation, $= L_q = E / E^{0.31}$. should be a dimensionless, ratio, and independent of mass. But since E is proportional to mass, we extend the Possenti relation, without loss of generality, to provide a mass scale invariant quantity. We therefore take $/ (E = m)^{0.31}$. From the Possenti correlation, assuming all the objects in their study have the canonical $m = 1.4$, we then find that

$$= 7 \cdot 10^4 (E = m)^{0.31} = 4.6 \cdot 10^4 (10^{-36} L_{c,2})^{0.31} \quad (47)$$

Since the magnetic moment, I , enters each of the above luminosity equations it can be eliminated from ratios of these luminosities, leaving relations involving only masses and spins. For known masses, the ratios then yield the spins. Alternatively, if the spin is known from burst oscillations, pulses or spectral determinations of r_c , one only needs one measured luminosity, L_c or L_m in at the end of the transition into the soft state, to enable calculation of the remaining I and L_q . In the case of G B H C modeled as M ECO, we found it to be necessary to estimate the co-rotation radius from multicolor disk fits to the thermal component of low state spectra. The reason for this is that the luminosities are sometimes unavailable across the whole spectral hardening transition from L_c to L_m in for G B H C. For G B H C, it is a common finding that the low state inner disk radius is much larger than that of the marginally stable orbit; e.g. Marko, Falcke & Fender 2001, Zdziak, Done & Smith 1997a,b 1998, Done & Zdziak 1999, Wilson & Done 2001]. The presence of a magnetosphere is an obvious explanation. Given an inner disk radius at the spectral state transition, the G B H C spin frequency follows from the Kepler relation $2\pi_s = GM/r^3$. Although we have taken our model and used it to predict the spin rates and accurate quiescent luminosities for NS and G B H C, it now appears that we could use the fact that the model fits well

to calculate more accurate parameters. By placing the last mass scale invariant Possenti relation for \dot{m} into the relation for quiescent luminosity and using it with the expression for L_c , we can determine spin rates to be given by

$$= 89 (L_{q;32} = (\dot{m} L_{c;36}^{1/31}))^{1/31} \text{ Hz} \quad (48)$$

where $L_{q;32} = 10^{-32} L_q$ and $L_{c;36} = 10^{-36} L_c$. Consistency of the above mass scaling equations also requires that the magnetic field equipartition condition must hold as

$$L_{c;36} = (\dot{m}^4)^{1/3} = 1 \quad (49)$$

Using the above equations the average spin rate for the G B H C is found to be 10 Hz and the average G B H C magnetic moment has the average value of 2200 gauss-cm³. Since this scaling technique essentially preserves the quiescent luminosities, the calculated results are more reliable than those obtained from determining the inner disk radii from spectral fitting.

16. Appendix 8 – Properties of The Low Hard State – Mass Ejection and Radio Emission

The radio flux, F , of jet sources has a power law dependence on frequency of the form

$$F \propto \nu^{-\alpha} \quad (50)$$

It is believed to originate in jet outflows and has been shown to be correlated with the low state x-ray luminosity [Meroni, Heinz & Di Matteo 2003], with $F \propto L_x^{0.7}$. The radio luminosity of a jet is a function of the rate at which the magnetosphere can do work on the inner ring of the disk. This depends on the relative speed between the magnetosphere and the inner disk; i.e., $E = (\dot{m}_s - \dot{m}_k)$, or

$$E = \left(\frac{r}{r_c}\right)^2 \frac{\dot{m}_s (1 - \frac{\dot{m}_k}{\dot{m}_s})}{r^3} / \left(2M \frac{3}{2} \dot{m}_{edd}^{6/7} \dot{m}_s (1 - \frac{\dot{m}_k}{\dot{m}_s})\right)^{1/2} \quad (51)$$

Here \dot{m}_{edd} is the mass accretion rate divided by the rate that would produce luminosity at the Eddington limit for mass M. Disk mass, spiraling in quasi-Keplerian orbits from negligible speed at radial infinity must regain at least as much energy as was radiated away in order to escape. For this to be provided by the magnetosphere requires $E = GM M = 2r$, from which $\dot{m}_k - 2\dot{m}_s = 3$. Thus the magnetosphere alone is incapable of completely ejecting all of the accreting matter once the inner disk reaches this limit and the radio luminosity will be comensurately reduced and ultimately cut off at maximum x-ray luminosity for

the low state and $\dot{M}_k = \dot{M}_s$. Typical data for GX 339-4 [Gallo, Fender & Pooley 2003] are shown in Figure 1. For very rapid inner disk transit through the co-rotation radius, fast relative motion between inner disk and magnetosphere can heat the inner disk plasma and strong bursts of radiation pressure from the central object may help to drive large outflows while an extended jet structure is still largely intact. This process has been calculated¹² using pressures and poloidal magnetic fields of unspecified origins. A MECO is obviously capable of supplying both the field and a radiation pressure. The hysteresis of the low/high and high/low state transitions may be associated with the need for the inner disk to be completely beyond the corotation radius before a jet can be regenerated after it has subsided. Since E_r / r^3 and $L_d / r^{9/2}$, it is apparent that we should expect radio luminosity, $L_R / L_d^{2/3}$. In particular we find

$$L_R = C(M; \dot{M}_s) 2L_c^{1/3} L_d^{2/3} (1 - \dot{M}_k / \dot{M}_s) \quad (52)$$

where $C(M; \dot{M}_s) = M^3$ and $C(M; \dot{M}_s)$ is a constant, dependent on the radio bandpass. It has been analyzed and evaluated [Robertson & Leiter 2004]. The cut-off at $\dot{M}_k = 1$ is shown by the line on Figure 1. The cut-off typically occurs with x-ray luminosity of 0.01–0.02 times Eddington luminosity. If we let $x = L_d/L_c$, then for $x < 1$, corresponding to the low state, then the above equations imply that:

$$L_R = C(M; \dot{M}_s) 2L_c (x^{2/3} - x) \quad (53)$$

The function has a maximum value of $0.3C(M; \dot{M}_s)L_c$ at $x = 0.3$. Strictly speaking, L_d , in these equations should be the bolometric luminosity of the disk, however, the x-ray luminosity over a large energy band is a very substantial fraction of the disk luminosity. To compare with the correlation exponent of 2/3 obtained here, recent studies, including noisy data for both GBC and AGN have yielded 0.71–0.01 [Gallo, Fender & Pooley 2003], 0.72 [Marko et al. 2003, Falcke, Kording & Marko 2003], 0.60–0.11 [Meroni, Heinz & Di Matteo 2003] and 0.64–0.09 [Maccarone, Gallo & Fender 2003]. For \dot{M}_s in the range (0 to -0.5), $L_R / M^{1/2}$, \dot{M}_s / M^{-1} and L_c / M , the MECO model yields $C(M) / M^{(9/4)^{1/2}}$ and (neglecting the cut-off region)

$$\log L_R = (2/3) \log L_x + (0.75 - 0.92) \log M + \text{const.} \quad (54)$$

which is a better fit to the "fundamental plane" of Meroni, Heinz & Di Matteo [2003] than any of the ADAF, disk/corona or disk/jet models they considered (see their Figure 5 for a \log^2 density plot). This last relation correctly describes the correlation for both

¹²though for inner disk radii inside the marginally stable orbit [Chou & Tajima 1999]

GBHC and AGN. In the low state, the inner disk radius is inside the light cylinder, with hot, diamagnetic plasma reshaping the magnetopause topology [Arons et al. 1984]. This magnetic propeller regime [Ilyin & Sunyaev 1975, Stella, White & Rosner 1986, Cui 1997, Zhang, Yu & Zhang 1997, Campana et al. 1998] exists until the inner disk pushes inside the co-rotation radius, r_c . From r_{lc} to r_c , the x-ray luminosity may increase by a factor of $10^3 - 10^6$. Inside r_c , large fractions of the accreting plasma can continue on to the central object and produce a spectral state switch to softer emissions. We have shown [Robertson & Leiter 2002] that magnetic moments and spin rates can be determined from luminosities at the end points of the transition from low/hard to high/soft spectral states. In that paper the magnetic moments and spins were used to calculate the $10^3 - 10^6$ times fainter quiescent luminosities expected from spin-down. During waning phases of nova outbursts, $L_c = 0.02L_{Edd}$ can be identified as the maximum disk luminosity upon entering the low state.

Until the inner disk reaches r_c , accreting plasma is ejected. It may depart in a jet, or as an outflow back over the disk as plasma is accelerated on outwardly curved or open magnetic field lines. Radio images of both flows have been seen [Paragi et al. 2002]. Equatorial outflows could contribute to the low state hard spectrum by bulk Comptonization of soft photons in the outflow, however, we think the hard spectrum originates primarily in patchy coronal areas [Meroni & Fabian 2002] on a conventional geometrically thin, optically thick disk consistent with the existence of a magnetic flux line breaking and reconnection process acting above the accretion disk.

17. Appendix 9 – The Existence and Stability of Highly Redshifted MECO

We have shown that the existence of AGN containing observable intrinsic magnetic moments is consistent with a new class of magnetospheric eternally collapsing object (MECO) solutions of the Einstein field equations of General Relativity. These solutions are based on a strict adherence to the SPE requirement for timelike world line completeness; i.e., that the world lines of physical matter under the influence of gravitational and non-gravitational forces must remain timelike in all regions of spacetime. Since there is nothing in the structure of the Einstein tensor, G , on the left hand side of the Einstein field equation that dynamically enforces 'timelike world line completeness', we have argued that the SPE constrains the physically acceptable choices of the energy momentum tensor, T to contain non-gravitational forces that can dynamically enforce it. In this context we have found the long-lived MECO solutions.

An enormous body of physics scholarship developed primarily over the last half century

has been built on the assumption that trapped surfaces leading to event horizons and curvature singularities exist. Misner, Thorne & Wheeler [1973], for example in Sec. 34.6 clearly state that this is an assumption and that it underlies the well-known singularity theorems of Hawking and Penrose. In contrast, we have found that strict adherence to the SPE demand for timelike world line completeness requires a 'no trapped surface condition'. This has led to the quasi-stable, high redshift MECO solutions of the Einstein field equations. The physical mechanism of their stable rate collapse is an Eddington balance maintained by the distributed photon generation of a highly compact and redshifted equipartition magnetic field. This field also serves to connect the pair plasma dominated outer layers of the MECO and the thin MECO pair atmosphere. Redshifts of $z = 10^8 (m=7)^{1/2}$ have been found to be necessary for compatibility with our previously found magnetic moments for GBC.

In this Appendix we give a detailed description of the MECO's properties. These properties can be shown to be compatible with standard gas pressure dominated 'alpha' accretion disks which is consistent with the fact (previously shown in Appendix 7 and 8) that the magnetosphere/disk interaction affects nearly all of the spectral characteristics of NS and GBC in LMXB systems and accounts for them in a unified and complete way, including jet formation and radio emissions. This model is solidly consistent with accreting NS systems, for which intrinsic magnetic moments obtained from spin-down measurements allow little choice. The magnetic fields are too strong to ignore. Since the similar characteristics of GBC are cleanly explained by the same model, the MECO offers a unified theory of LMXB phenomenology as well as extensions to AGN. Since MECO lifetimes are orders of magnitude greater than a Hubble time, they provide an elegant and unified framework for understanding the broad range of observations associated with GBC and AGN. Lastly we have indicated some ways in which the existence of MECO in GBC and AGN might be detected and confirmed.

A MECO is, in many ways, more exotic than a black hole with its mere mass and spin. It is equally compact but its surface magnetic field is sufficient to produce pairs from the quantum electrodynamical vacuum. This occurs at a threshold that is insensitive to mass, thus MECO can range in mass from galactic black hole candidates GBC to active galactic nuclei AGN. The scaling with mass of the distantly observed magnetic fields, $B / M^{1/2}$ allows the ratio $L_c = L_{Edd}$ to also be mass scale invariant [Robertson & Leiter 2004]. The MECO interior magnetic fields are relatively modest. Interior and surface fields differ due to substantial pair drift currents on the MECO surface. In general, plasmas in hydrostatic equilibrium in magnetic and gravitational fields experience drift currents proportional to $g B = B^2$. The general relativistic generalization of this provides the key to our understanding of the high redshifts of MECO.

The surface temperature and high luminosity to radius ratio (hereafter L/R) compactness, (see Appendix 10). of the MECO Eddington limited, timelike, secular collapsing state implies that the plasma is dominated by electron-positron pairs. These are generated by colliding photons due to the optically thick synchrotron luminosity of the intrinsic MECO magnetic field, both within the interior and on the MECO surface. Recall that the surface is well inside the photon orbit and the bulk of the photon outflow from the surface falls back. The existence of the MECO state requires that:

$$L_{Edd}(\text{outflow}) = L_{Syn}(\text{out}) \quad (55)$$

within the MECO and

$$L_{Edd,S}(\text{escape}) = L_{Syn,S}(\text{escape}) \quad (56)$$

at the MECO surface S . We have (see Appendix 4)

$$L_{Edd,S}(\text{escape}) = (4 \pi G M_s / c) (1 + z_s) = 1.3 \times 10^{38} m (1 + z_s) \quad (57)$$

$$L_{Syn,S}(\text{escape}) = L_{Syn,S}(\text{out}) = (4 = 27) (1 + z_s)^2 \quad (58)$$

Assuming a temperature near the pair production threshold, the rate of synchrotron photon energy generation in a plasma containing N electrons and positrons is [Shapiro & Teukolsky 1983]

$$L_{Sync,S}(\text{out}) = (16 e^4 / 3 m_e c^3) N B^2 (T_9 = 6)^2 = 1.27 \times 10^{14} N B^2 (T_9 = 6)^2 \text{ erg/s} \quad (59)$$

where $T_9 = 10^9 T$ and $T_9 = 6 = kT / m_e c^2$. For an Eddington equilibrium, we require the synchrotron generation rate to produce the outflow through the MECO surface. Thus

$$L_{Edd}(\text{out}) = 1.27 \times 10^{38} m (4 (1 + z_s)^3 = 27) = 1.27 \times 10^{14} N B^2 (T_9 = 6)^2 \text{ erg/s} \quad (60)$$

which implies that

$$N B^2 = 10^{52} (m = 7) (1 + z_s)^3 (6 = T_9)^2 \text{ erg/cm}^3 \quad (61)$$

From Section 6 of Baumgarte & Shapiro [2003], we note that if m is the distantly observed MECO magnetic moment and $(1 + z_s) \gg 1$ is the MECO surface redshift, then the Einstein-Maxwell equations imply that the components of the MECO dipole magnetic field strength, B at distance r are given by

$$B_r = 2F(x) \cos(\theta) = r^3 \quad (62)$$

and

$$B_\theta = G(x) \sin(\theta) = r^3 \quad (63)$$

where $x = r_s/2R_g$ and

$$F(x) = (3x^3)(\ln(1-x^{-1}) + x^{-1}(1+x^{-1})^{-2}) \quad (64)$$

$$G(x) = (6x^3)((1-x^{-1})^{1/2}\ln(1-x^{-1}) + x^{-1}(1+x^{-1})^{-2}(1-x^{-1})^{-1/2}) \quad (65)$$

Note that for $r_s \gg 2R_g$, $x \gg 1$ and both $F(x)$ and $G(x) \approx 1$, while as we approach a compact MECO surface where $(1+z_s) \gg 1$, then $x \approx 1$ and

$$F(x) \approx 3\ln(1-x^{-1}) = 3\ln(1=(1+z_s)^2) = 6\ln(1+z_s) \quad (66)$$

and

$$G(x) \approx 3(1-x^{-1})^{1/2} = 3(1+z_s) \quad (67)$$

Hence the radial component of the magnetic field on the MECO surface is given by

$$B_{r;s^+} = 12\ln(1+z_s) \cos(\theta) = (2R_g)^3 \quad (68)$$

while the poloidal component is given by

$$B_{\theta;s^+} = 3(1+z_s) \sin(\theta) = (2R_g)^3 \quad (69)$$

The interior magnetic dipole fields, B^0 in the MECO, which are due to the interior MECO magnetic dipole moment (r) in the interior will be given by

$$B_r^0 = 6(r) \cos(\theta) \ln(1+z) = r^3 \quad (70)$$

and

$$B_\theta^0 = 3(r) \ln(1+z) \sin(\theta) = r^3 \quad (71)$$

Thus the expressions for the exterior magnetic field just outside of the MECO surface differ by the factors $F(x_s)$ and $G(x_s)$ from those of the interior magnetic field. But these general relativistic expressions imply important consequences because

(a) The general relativistic structure of the Maxwell-Einstein equations causes the radial and poloidal exterior components of the MECO magnetic dipole fields to undergo redshift effects which are different functions of $(1+z_s)$

and

(b) The radial component $B_{r;s}$ of the magnetic dipole field is continuous at the MECO surface, but the poloidal component is not. $B_{\theta;s^+}$ is different from $B_{\theta;s}^0$ at the MECO surface.

This difference is caused by powerful drift currents that are induced by the strong gravitational field and enhanced by the differing general relativistic dependence on

redshift of the poloidal and radial magnetic field components. This is a general relativistic generalization of the fact that a plasma in hydrostatic equilibrium in gravitational and magnetic fields experiences drift currents proportional to $g \cdot B = B^2$. In fact, it is the drift currents that generate the distantly observed magnetic moments seen in MECO-GBH C and MECO-AGN.

The MECO magnetic moment coupling to a surrounding accretion disk will cause it to be a slow rotator. Hence to estimate the strength of the magnetic field just under the surface of the MECO of the GBC we can use the results obtained for low redshift, slowly rotating compact stellar objects with magnetic fields. The magnetic field strength in the interior of a slowly rotating neutron star of radius 10 km, was shown to be $10^{13.7}$ G [Gupta, Mishra, Mishra & Prasanna 1998]. When scaled to the $7M$ and $R = 2R_g$ size of the MECO, the magnetic fields under the surface can be estimated to be (neglecting latitude angle dependence):

$$B_{r,S} = (2 = (2R_g)^3) 6 \ln(1 + z_s) (10^{13.7} \text{ gauss}) = (M = 7M)^{1/2} \quad (72)$$

$$B_{s,S} = (= (2R_g)^3) 6 \ln(1 + z_s) (10^{13.4} \text{ gauss}) = (M = 7M)^{1/2} \quad (73)$$

Then from Eqs (66)–(73), the exterior magnetic fields on the MECO surface S are:

$$B_{r,S+} = B_{r,S} (2 = (2R_g)^3) 6 \ln(1 + z_s) \cos(\phi) (10^{13.7} \text{ gauss}) \cos(\phi) = (M = 7M)^{1/2} \quad (74)$$

$$B_{s,S+} = (= (2R_g)^3) 3 (1 + z_s) \sin(\phi) \quad (75)$$

Using these equations, the magnitude of the surface redshift $(1 + z_s)$ for a MECO can be directly determined by noting that the strength of the poloidal component of the equipartition magnetic field $B_{r,S}$ on the MECO surface must be the same for all MECO's (i.e. it must be mass scale invariant since it cannot be locally much larger than the quantum electrodynamically determined maximum value for a NS given by $B_{r,S} = 10^{20}$ gauss [Harding, A., 2003]). This is because surface magnetic fields much larger than 10^{20} gauss would create a spontaneous quantum electrodynamic phase transition associated with the vacuum production of bound pairs on the MECO surface [Zaumen 1976]. This would cause more pairs to be produced than those required by the Eddington balance of the MECO surface. This would then cause the MECO surface to expand. However the resultant expansion due to this process would reduce the redshift and the surface poloidal magnetic field thus quenching the vacuum production of bound pairs and allowing the MECO surface to contract. This stability mechanism on the MECO surface implies that its surface redshift $(1 + z_s)$ can be dynamically determined from the preceding pair of equations. Neglecting the trigonometric functions common to both sides of the equations, the ratio of these external field components in Eqs. (69) and (71), yields

$$3(1 + z_s) = [6 \ln(1 + z_s)] 10^{20} = [10^{13.4} = (M = 7)^{1/2}] \quad (76)$$

for which the solution is

$$(1 + z_s) = 1.5 \times 10^8 (m=7)^{1/2} \quad (77)$$

In addition we obtain

$$= (2R_g)^3 (2.2 \times 10^{11} \text{ gauss}) = (m=7)^{1/2} \quad (78)$$

which implies that the average distantly observed intrinsic magnetic moment of the M ECO is

$$(2 \times 10^{30} \text{ gauss cm}^3) (m=7)^{5/2} \quad (79)$$

This is in good agreement with our analysis of observations. From the above equations we can now get a rough estimate of the pair density, by considering the N to be uniformly distributed over a volume of $4(1 + z_s)(2R_g)^3 = 3$ and by considering the interior magnetic field to be uniform at $2.5 \times 10^{13} (m=7)^{1/2}$ gauss. Hence

$$n = 10^{22} (m=7)^{3/2} (6=T_g)^2 = \text{cm}^{-3} \quad (80)$$

which for a G B H C , agrees within a factor of two of the result found for a pair plasma at

$T = 6 \times 10^9 \text{ K}$. This result for n implies that surface temperature would increase with increasing mass, however, it only increases by a factor of 10 for $m = 10^8$. Since mean M ECO densities scale as $1=m^2$, one might expect larger density gradients and different ratios of pairs to neutrons and protons in AGN compared to G B H C , which are approximately of nuclear densities. A significant M ECO surface currents are the source of the distantly observed magnetic moment seen in the M ECO -G B H C . The magnitude of these surface currents is essentially mass scale invariant and is given by

$$i(S) = (c=4) (= (2R_g)^3) \beta (1 + z_s) \sin(\theta) = 3.3 \times 10^{26} \text{ amp} \quad (81)$$

total current on G B H C surface, which corresponds to

$$2 \times 10^{45} \text{ e}^{-} \text{ sec} \quad (82)$$

combined surface $e^+ - e^-$ flow. Hence the above equations imply that the corresponding drift speeds of electrons and positrons are $v=c/1$. This implies that the opposed $e^+ - e^-$ pairs currents on the M ECO surface are moving relativistically and hence will have a very long lifetime before annihilating. This maintains a stable flow of current as required to generate the distantly observed M ECO magnetic moments. The radiation pressure at the outer surface of the M ECO is

$$P_{\text{Syn}}(\text{out}) = L_{\text{Syn}}(\text{out}) = [4(2R_g)^2 c] = 2.7 \times 10^{38} (m=7)^{1/2} \text{ erg cm}^{-3} \quad (83)$$

For comparison, the mass-energy density of a M ECO is

$$\rho = M c^2 = [(1 + z_s) 4 \pi (2R_g)^3 / 3] = 2 \times 10^{27} \text{ g/cm}^3 \quad (84)$$

which suggests that M ECO is radiation dominated and very tightly gravitationally bound.

An order of magnitude calculation of binding energy ¹³ yields $1.5M c^2 \ln(1 + z_s)$ for a residual mass, M . Thus the progenitor of a M ECO -GBHC would have a mass of 200–300 M_\odot , and this suggests that they would be among the earliest and most massive stars in the galaxy. On the other hand the progenitor of a $10^9 M_\odot$ M ECO -AGN with its very large intrinsic magnetic moment would most likely originate from the collapse of magnetized plasma containing angular momentum in addition to aggregates of primordial planetoids, like that discussed in section 5 of this paper, with a total mass of $4 \times 10^{10} M_\odot$.

18. Appendix 10 – The + \$ e Phase Transition and M ECO Existence

It is well-known that a spherical volume of radius R containing a luminosity L of gamma ray photons with energies $> 1 \text{ MeV}$, ¹⁴ will become optically thick to the $+ e$ process when

$$n R \approx 1 \quad (85)$$

and

$$n L = (2 \pi R^2 m_e c^3) \quad (86)$$

is the number density of γ -ray photons with energies $> 1 \text{ MeV}$, L is the gamma-ray luminosity, R is the radius of the volume, and σ_T is the pair production cross section. Since $\sigma_T \approx 10^{-28} \text{ cm}^2$ near threshold, it follows that the system becomes optically thick to photon-photon pair production when the numerical value of its compactness parameter L/R is

$$L/R = 4 \pi m_e c^3 / \sigma_T = 5 \times 10^{29} \text{ erg/cm sec} \quad (87)$$

Hence $L/R > 1$ will be satisfied for systems with compactness

$$L/R > 10^{30} \text{ erg/cm sec} \quad (88)$$

¹³This has obvious, important consequences for hypernova models of gamma-ray bursters.

¹⁴1 MeV photons correspond to $T = 10^{10} \text{ K}$, which is only slightly beyond the pair threshold, and easily within reach in gravitational collapse.

For an Eddington limited MECO, which has a very large surface redshift $(1+z) \gg 1$ at $R = 2R_g$, and taking the proper length and volume into consideration, the optical depth to photon-photon pair production has the very large value

$$(1+z) \quad (L_{;30}=R) \quad 10^2 \quad (1+z)^3 \gg 1 \text{ erg/cm sec} \quad (89)$$

Thus the resultant + \$ e phase transition in the MECO magnetic field, B_s , creates an optically thick pair dominated plasma. Taking the photon escape cone factor $1=(1+z)^2$ into account, the process generates a net outward non-polytropic radiation pressure

$$P = (1+z)B_s^4 m \quad (90)$$

on the MECO surface. The increase of pressure with redshift is a key feature of the Eddington limited secular balance at $R = 2GM=c^2$. Thus trapped surfaces, which lead to event horizons, can be prevented from forming. As discussed in Appendix 9 above, the balance is mass scale invariantly stabilized at the threshold of magnetically produced pair breakdown of the vacuum.

R E F E R E N C E S

Abrams, L. S., 1979 *Phys. Rev. D* 20, 2474

Abrams, L. S., 1989 *Can. J. Phys.* 67, 919, gr-qc/0102051

Arons, J. et al. 1984 in *High Energy Transients in Astrophysics*, *AIIP Conf. Proc.* 115, 215, Ed. S. W. Woosley, Santa Cruz, CA

Baumgarte, T. & Shapiro, S. 2003 *ApJ* 585, 930

Bhattacharya, D. & Srinivasan, G., 1995 in *X-Ray Binaries*, eds W. Lewin, J. van Paradijs & E. van den Heuvel, Cambridge Univ. Press

Campana, S. et al., 2002 *ApJ* 580, 389

Campana, S. et al., 1998 *A & A Rev.* 8, 279

Chou & Tajima 1999 *ApJ* 513, 401

Colley, W. & Schild, R., 1999, *ApJ*, 518, 153

Colley, W. & Schild, R., 2000, *ApJ*, 540, 104

Colley, W. & Schild, R., 2003, *ApJ*, 594, 97 (CS03)

Colley, W. et al., 2003, *ApJ*, 587, 71

Cui, W. 1997 *ApJ* 482, L163

De Vries et al., 2005, *AJ*, 129, 615

Diemand, J., Moore, B. & Stadel, J., 2005, *Nature*, 433, 389

Done, C. & Zdziarski, P. 1999 *MNRAS* 305, 457

Elvis, M., 2000, *ApJ*, 545, 63

Elvis, M. et al., 1994, *ApJ Supplements*, 95, 1

Gallop, E., Fender, R., Pooley, G., 2003 *MNRAS*, 344, 60

Ghosh, P. & Lamb, F. 1992 in *X-Ray Binaries and Recycled Pulsars*, Ed. E. van den Heuvel and S. Rappaport, Kluwer

Gibson, C. 1996, *Applied Mechanics review*, 49 299; astro-ph/9904260

Gibson, C. 1999, astro-ph/9904260

Gieveon, U. et al, 1999, MNRAS, 306, 637

Goodson, A., Bohm, K. & Winglee, R. 1999 ApJ 534, 142

Gould, A. and Miralde-Escude, J., 1997, ApJ, 483, 13

Gupta, A., Mishra, A., Mishra, H., & Prasanna, A.R., 1998, Classical and Quantum Gravity, 15, 3131

Haarsma, D. et al, 1997, ApJ, 479, 102

Haarsma, D. et al, 1999, ApJ, 510, 64

Harding, A., 2003, Invited talk at Pulsars, AXPs and SGRs Observed with BeppoSAX and Other Observatories, Marsala, Sicily, Sept. 2002 astro-ph/0304120.

Hawkins, M. 1996, MNRAS, 278, 787

Hawley, J., Balbus, S. & Winters, W., 1999 ApJ 518, 394

Hernandez Jr., W.C. & Misner, C.W., 1966 ApJ. 143, 452

Hill, A. et al, 2004, astro-ph/0411752

Igumenschev, I.Narayan, R. and Abramowicz, M., 2003, ApJ, 592, 1042

Ivanov, A. & Sunyaev, R. 1975 A&A 39, 185

Kato, Y., Hayashi, M., Matsumoto, R. 2004 ApJ in press astro-ph/0308437

Koopmans, L. et al, 2003, ApJ, 595, 712

Lehar, J. et al, 1992, ApJ, 384, 453

Leiter, D. and Robertson, S. 2003, Found. Physics Lett. 16, 143

Lindquist, R.W., Schwartz, R.A. & Misner, C.W. 1965 Phys. Rev., 137B, 1364.

Lindquist, R.W., 1966 Annals of Physics, 37, 487

Macarone, T., Gallo, E., Fender, R. 2003 MNRAS 345, L19

Marko, S., Falcke, H., & Fender, R. 2001 A&AL 372, 25

Marko, S., Nowak, M., Corbel, S., Fender, R., Falcke, H., 2003 New Astron. Rev. 47, 491

Matt, S., Goodson, A., Winglee, R., Bohm, K. 2002 ApJ 574, 232

Merloni, A., Fabian, A., 2002 MNRAS, 332, 165

Merloni, A., Heinz, S., Di Matteo, T., 2003 MNRAS, 345, 1057

Misner, C. W. 1965 Phys. Rev., 137B, 1360 2005-4-20rudy_le009.jpg

Misner, C., Thorne, K. & Wheeler, J. 1973 'Gravitation', Freeman, San Francisco, California

Mitra, A. 1998 ApJ 499, 385

Mitra, A. 2000 Found. Phys. Lett. 13, 543

Mitra, A., 2002 Found. Phys. Lett. 15, 439

Narayan, R. and Quataert, E. 2005, Science, 307, 77

Oscoz, A. et al 2001, ApJ, 552, 81

Paragi, Z., et al. 2002 Talk presented at the 4th Microquasar Workshop, Cargese, Corsica
May 27-31 astro-ph/0208125

Pelletier, G. & Marcowith, A., 1998 ApJ 502, 598

Pelt, J. et al, 1996, A&A, 305, 97

Pelt, J. et al, 1998, A&A, 336, 829

Pijpers, F. 1997, MNRAS, 289, 933

Possenti, A., Cenutti, R., Colpi, M., & Mereghetti, S. 2002 A&A 387, 993

Press, W. et al, 1992, ApJ, 385, 404

Putman, M. and Moore, B. 2002, in Extragalactic Gas at Low Redshift; A SP Conference Proceedings 254, ed. J. Mulchaey and John Stocke [San Francisco: Astronomical Society of the Pacific] p. 245

Rauch, K. and Blandford, R., 1991, ApJ, 381, 39

Refsdal, S., and Stabell, R. 1991, A&A, 250, 62

Refsdal, S., and Stabell, R. 1993, A&A, 278, L5

Refsdal, S., and Stabell, R. 1997, A&A, 325, 877

Reid, M . et al., 2003 ApJ 587, 208

Robertson, S ., and Leiter, D . 2002, ApJ, 565, 447

Robertson, S ., and Leiter, D . 2003, ApJ, 596, L203

Robertson, S ., and Leiter, D . 2004, MNRAS, 350, 1391

Romanova, M . et al, 2002, ApJ, 578, 420

Romanova, M . et al, 2003a, ApJ, 588, 400

Romanova, M . et al, 2003b, ApJ, 595, 1009

Romanova, M . et al, 2004, ApJ, 616, L151

Schild, R ., 1990, AJ, 100, 1991

Schild, R . E . 1996, ApJ, 464, 125

Schild, R . E . 1999, ApJ, 514, 598

Schild, R . E . 2004, astro-ph/0409549

Schild, R . E . 2005, AJ, 129, 1225

Schild, R . E ., & Choln, B . 1986, ApJ, 300, 209

Schild, R . E ., & Smith, R . C ., 1991, AJ, 101, 813

Schild, R . E ., & Thompson, D . J., 1995, AJ, 109, 1970

Schild, R . and Thompson, D . J. 1997, AJ, 113, 130

Schild, R . E ., & Thompson, D . J., 1997a, AJ, 113, 130

Schild, R . E ., & Thompson, D . J. 1997b, in *Astronomical Time Series*, ed. D . Maoz, A . Sternberg, and E . Liebowitz [Boston: Kluwer] p. 74 D . J., 1995, in *Dark Matter: AIP S .Holt & C .Bennett AIP Press*:

Schild, R . E ., & Vakulik, V ., 2003, AJ, 126, 689 (SV 03)

Thompson, D . J., & Schild, R ., 1997,, in *Applications of Time Series Analysis in Astronomy and Meteorology*, ed. T . Subba Rao, M . Priestly, & O . Lessi [Chapman and Hall: New York], 187

Shapiro, S. & Teukolsky, S. 1983 in *Black Holes, White Dwarfs & Neutron Stars*, John Wiley & Sons, Inc., New York

Spekkens, K., Giovanelli, R. and Haynes, M. 2005, AJ, 129, 2119

Stella, L., White, N. & Rosner, R. 1986 ApJ 308, 669

Thorne, K., 1965 Phys. Rev., 138, B251

Uzdensky, D., 2002 ApJ 572, 432

Walker, M. and Wardle, M., 1998, ApJ, 498, 125

Wardle, M. and Walker, M., 1999, ApJ, 527, 109

Wheeler, J. & Ciufolini, I., 1995 in *Gravitation And Inertia* Princeton Univ. Press, 41 William St., Princeton, New Jersey

White, N. & Marshall, F. 1984, ApJ. 281, 354

Wilson, C. & Done, C. 2001 MNRAS 325, 167

Winn, J. et al, 2004, AJ, 128, 2696

Zaumen, W. T., 1976 ApJ, 210, 776

Zhang, W., Yu, W. & Zhang, S. 1998 ApJ 494, L71

Zycki, P., Done, C. and Smith, D. 1997a in AIP Conf. Proc. 431, *Accretion Processes in Astrophysical Systems: Some Like It Hot*, Ed. S. S. Holt & T. R. Kallman (New York, AIP), 319

Zycki, P., Done, C. and Smith 1997b ApJ 488, L113

Empirical Q0957 Structure

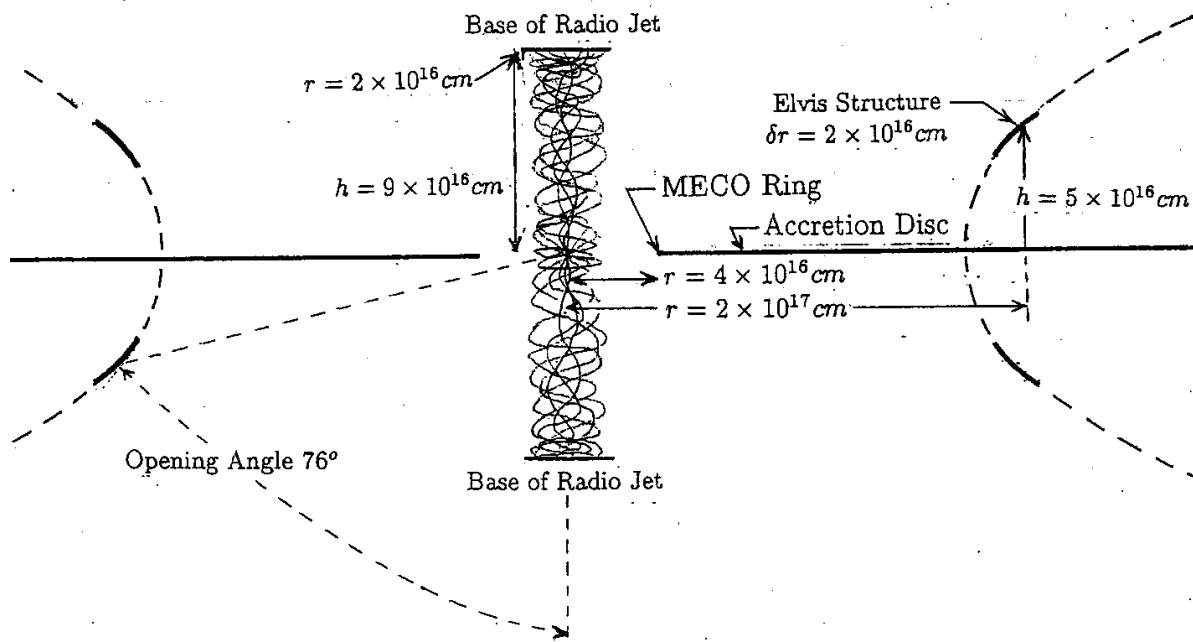


Fig. 1. A cartoon showing the principal structures in the empirical quasar model and specifying the size scales of the structures found, expressed in centimeters. In this cross-sectional view, the outer Elvis outflow structures must be understood as a section of the surfaces of revolution, and the luminous portions are shown as solid line segments. These have been modeled as circles in the Schild-Vakulik (2003) simulations. The inner luminous edge of the accretion disc, marked MECO ring, has a very high surface brightness, and is found to be outside an unexpectedly large empty inner region. The tangled magnetic field lines are shown only to the base of the radio jet. The overall geometry and proportions correspond closely to the rotating magnetic star models of Romano et al (2002, 2003a).

MAGNETOSPHERIC ETERNALLY COLLAPSING OBJECT (MECO) INSIDE OF THE QUASAR Q0957

(MECO) -----> THE SCHILD-VAKULIK STRUCTURE

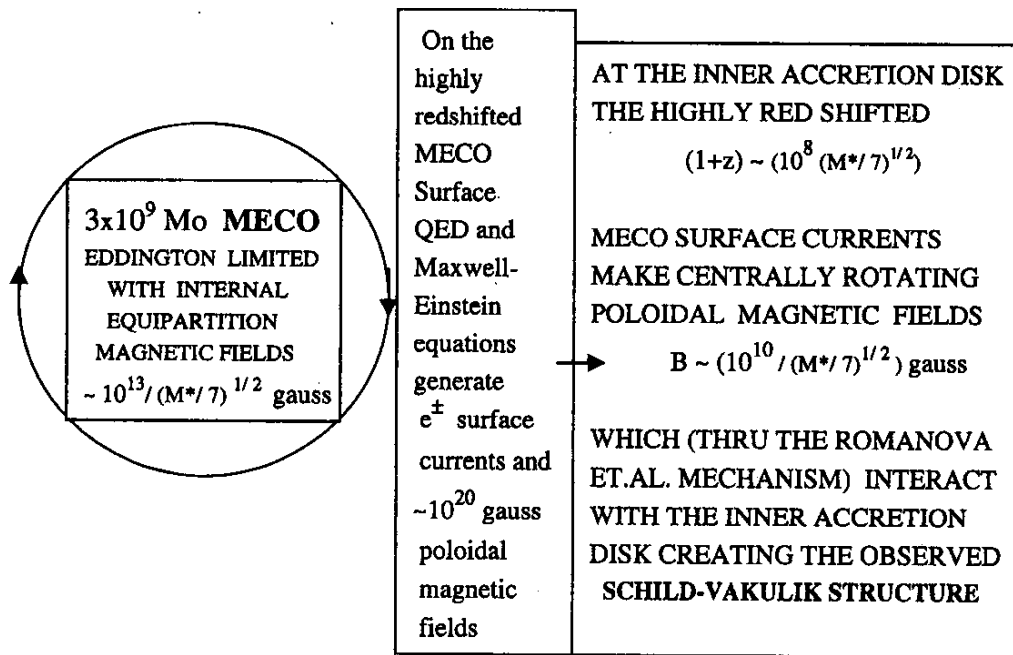


Fig. 2.1 A logic diagram to show how the Magnetospheric Eternally Collapsing Object (MECO) picture of physical quasar structure has been applied to the empirical quasar structure picture of Schild & Vakulik (2003). The rotating central object with Eddington limited internal equipartition magnetic fields generates surface currents and rotating poloidal magnetic fields that clear out the inner quasar region. The central rotating fields in the low-hard state interact with the inner edge of the accretion disc to produce the high surface brightness band at the inner accretion disc edge. The magnetic fields operating through the coronal region through the Romanova et al (2002, 2003a) interaction create the outer Elvis outflow structures simulated in SV03.